Large-scale mass transports, water mass formation, and diffusivities estimated from World Ocean Circulation Experiment (WOCE) hydrographic data

Alexandre Ganachaud

Institut de Recherche pour le Développement, Laboratoire d'Etudes Géophysiques et d'Océautographie Spatiale, Nouméa, New Caledonia

[1]   A global inversion is used to estimate the oceanic mass transports and vertical diffusivities based on a subset of hydrographic data from the World Ocean Circulation Experiment (WOCE) and Java Australia Dynamic Experiment. The analysis is based on the linear inverse "box" model of *Ganachaud and Wunsch* [2000] that consistently combines the transoceanic sections. A globally consistent solution is obtained for a depth-independent adjustment to the thermal wind field, the freshwater flux divergences, the Ekman transport, and the advective and diffusive dianeutral fluxes between layers. A detailed error budget permits calculation of statistical uncertainties, taking into account both the nonresolved part of the solution and the systematic errors due to the temporal oceanic variability. The horizontal structure of the transports for different density classes is analyzed regionally. During the WOCE period (1985–1996), net meridional transports are estimated, with 16 ± 2 Sv (10^6 m^3/s) of North Atlantic Deep Water (NADW) being produced in the northern North Atlantic, moving southward, entraining Antarctic Bottom Water (AABW), and Antarctic Intermediate Water increasing in volume transport to 23 ± 3 Sv at 30°S. In the Southern Ocean, 21 ± 6 Sv of bottom water was formed from lower Circumpolar Deep Water, which corresponds approximately to the lower NADW density range. Bottom water inflows (NADW + AABW mixture) to the Atlantic, Indian, and Pacific Oceans are estimated at 6 ± 1.3, 11 ± 4, and 7 ± 2 Sv, respectively. In the Indian and Pacific Oceans this water returns southward at deep and intermediate levels. Property anomaly conservation constraints permit estimation of dianeutral diffusivities in deep layers, with a global average of 3.7 ± 0.7 cm^{2}s^{-1} north of 30°S.   *INDEX TERMS:* 4532 Oceanography: Physical: General circulation; 4223 Oceanography: General: Descriptive and regional oceanography; 4283 Oceanography: General: Water masses; 4576 Oceanography: Physical: Western boundary currents; 4215 Oceanography: General: Climate and interannual variability (3309); *KEYWORDS:* transports, diffusivities, climate, Circumpolar Deep Water (CDW), WOCE, hydrographic

1.   Introduction

[2]   A quantitative determination of oceanic transports and mixing was one of the main objectives of the World Ocean Circulation Experiment (WOCE). In this paper, we present a global circulation scheme and vertical diffusivities from the transoceanic WOCE hydrographic sections that is consistent with ocean dynamics and simple biology and geochemistry. We examine the regional aspects of the global the circulation presented by *Ganachaud and Wunsch* [2000], who first attempted to use the WOCE sections in a global and consistent framework. Mass transport is the most basic element of the circulation that we focus on; heat and nutrient transport estimates were published independently [*Ganachaud et al.*, 2000; *Ganachaud and Wunsch*, 2003]. This work follows the tracks of *Macdonald and Wunsch* [1996], who used historical hydrographic data spanning 25 years to estimate a globally consistent circulation. In addition to the use of the high-quality hydrographic WOCE sections, several methodological improvements are made including a more quantitative estimate of absolute uncertainties [*Ganachaud*, 2003]. Our transports are compared with regional estimates and a semiquantitative picture of the global circulation [*Schmitz*, 1996]. The remaining uncertainties are discussed, suggesting modifications for future observations and methodologies.

2.   Method

[3]   A subset of WOCE transoceanic sections was used (Figure 1) to ensure temporal homogeneity and avoid
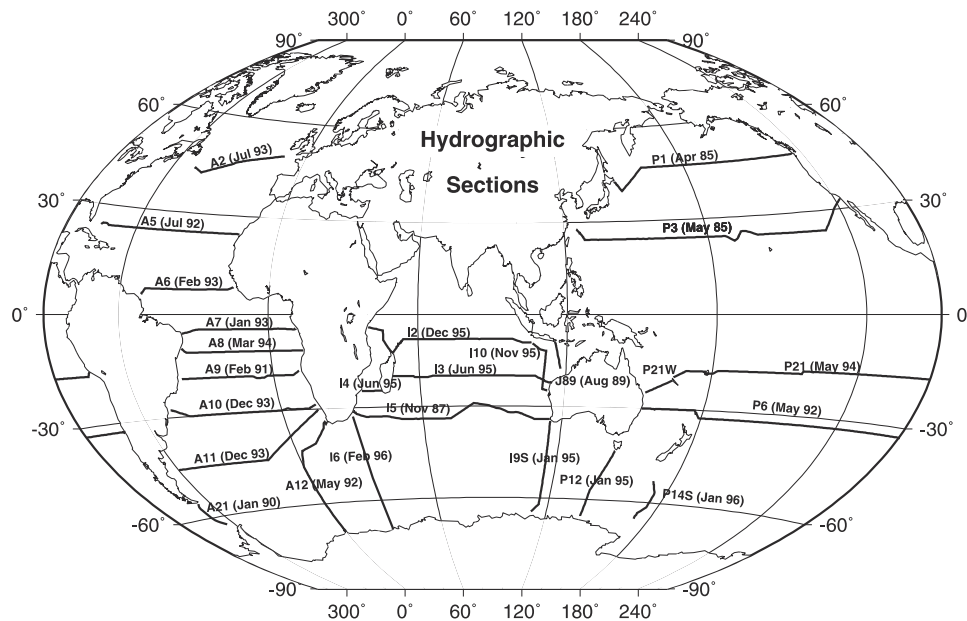
Figure 1. Selected WOCE and JADE hydrographic sections covering the period 1985–1996.

crossing sections which can introduce large biases in property budgets [e.g., *Wunsch and Grant*, 1982]. The sections are essentially zonal away from the Southern Ocean. Given the data, the model solution, at best, represents an average of the circulation for the 1989–1996 period in most oceans, except in the North Pacific where the sections were taken earlier, in 1985. The inverse methods provide convenient tools to obtain an ocean circulation that obeys simple conservation statements. Since the pioneering works of *Riley* [1951] and *Wunsch* [1978], steady geostrophic box inversions have been extensively used in most oceanic regions [e.g., *Wunsch*, 1996]. Linear inverse models allow transport computations at the high resolution of hydrographic sections with realistic error bars. However, they include additional uncertainties due to the inability to adjust density [see *Ganachaud*, 2003]. Alternative approaches are possible (e.g., a steady numerical model fit to climatological data) [*de las Heras and Schlitzer*, 1999], generally at the expense of uncertainty computation (model errors are inaccessible in the latter case).

[4] Using the basic procedure of the steady geostrophic box inversions [*Wunsch*, 1996], hydrographic and wind stress data are combined with geostrophic dynamics and prior knowledge of the solution elements (size of reference velocities; dianeutral transports and diffusivities; adjustments to Ekman transports and freshwater fluxes). Aside from the use of the WOCE data, the main improvements are:

[5] 1. Use of neutral surfaces instead of isopycnals [*Jackett and McDougall*, 1997], with calculation, as part of the inversion, of dianeutral transfers, dianeutral mixing of tracers [*Wijffels*, 1993], and freshwater fluxes, along with the reference velocities and ageostrophic transport adjustment in the surface layers (ascribed to a correction to Ekman transports).

[6] 2. Use of a more quantitative error budget derived from analysis of the impact of internal wave noise and oceanic variability on transport calculations [*Ganachaud*, 2003].

[7] 3. Property anomaly formulation for conservation equations [*Mcdougall*, 1991] based upon making explicit the necessary assumptions concerning the error covariance between mass constraints and property constraints [*Wunsch*, 1996, p. 273].

[8] 4. Use of National Center for Environmental Prediction (NCEP) reanalysis for the mean wind fields [*Kalnay et al.*, 1996] (Appendix C).

[9] 5. Determination and analysis of nutrient and oxygen divergences as part of the inversion [*Ganachaud and Wunsch*, 2003c].

[10] The flow is required to conserve approximately several properties (Table 1). Bulk advective ($w*$) and diffusive ($\kappa*$) transfers are allowed between layers (hereinafter referred to as dianeutral transfers). By definition there is no diffusion in the mass equation. Top-to-bottom silica is conserved within the bounds derived by *Ganachaud* [2003]. The anomaly equations for the conservative tracer "NO" ($9.1 \times NO_3 + O_2$ [*Broecker*, 1974] are, in general, indistinguishable from the "PO" equations and only the latter was constrained because the nitrogen cycle is the more complex one. A priori weights attributed to mass conservation equations are based on *Ganachaud* [2003] and extrapolated to the global ocean (Table 2). The weights on tracer conservation equations are set using the ad-hoc method of *Ganachaud et al.* [2000, Appendix A]. Constraints that are specific to each ocean are listed at the beginning of each of the following sections. The full inversion requires solving a 1200 equation system with 3000 unknowns. The solution is obtained using the Gauss-Markov estimator [*Wunsch*, 1996, p.184] that produces a minimum error variance solution. The posterior error covariance includes the part that is not resolved by the equations, in contrast with the conventional least squares or singular value decomposition estimators. A number of solutions were explored by changing the model configuration, and focusing on large-scale features such as the overturning circulation. A standard, or preferred solution is presented here, and selected alternative solutions are discussed.

Table 1. Conservation Constraints for the Standard Solution[a]

	Top-to-Bottom	Individual Layers
Mass	yes	yes
Heat[b]	no	below surface[c]
Salinity[b]	yes	yes
Silica[d]	yes	no
NO (9.1 NO_3 + O_2)	no	no
PO (170 PO_4 + O_2)[b,e]	no	below surface[c]

[a]From *Ganachaud et al.* [2000]. Lateral and dianeutral transports included.

[b]Anomaly formulation for heat, salinity, and "PO".

[c]Outcropping layers (or layers within 50 dbars of the surface) are nonconservative because of heat and oxygen exchanges with the atmosphere.

[d]The anomaly formulation was not used for silica for technical reasons [*Ganachaud*, 1999, p 24].

[e]From *Anderson and Sarmiento* [1994]; an experiment with a lower ratio of 140 [*Redfield et al.*, 1963] showed little change to the circulation.

[11] The flow was not explicitly constrained to force the net layer fluxes to be advected away from their supposed sources, although water mass distributions guided the choice of the "first guess" circulation. Away from the core of boundary currents, the mean mass flux direction does not always coincide with the direction implied by the mean property tongues, and given the existence of an eddy field and its potential effects on property distributions, the only reasonable constraints appeared to be enforcement of near-conservation of properties on the large scale. The uncertainty due to the arbitrary choice of a reference surface (or "first guess" circulation) is included by choosing the appropriate a priori size (or "range of adjustment") of the reference velocities. The solution is examined in each ocean, starting with the Atlantic.

3. Atlantic Ocean

[12] Qualitative pictures of the North Atlantic circulation and its connection with other basins have emerged from water mass analysis and current meter measurements by [*Reid*, 1994, 1996]. Elements of this large-scale circulation have been estimated more quantitatively with the help of inverse box models (*Wunsch* [1978], western North Atlantic; *Wunsch and Grant* [1982], whole North Atlantic; *Hall and Bryden* [1982], 24N; and *Roemmich and Wunsch* [1985] and *Rintoul and Wunsch* [1991], subtropical North Atlantic). In the South Atlantic, the circulation was estimated by *Fu* [1986] and *Lux and Mercier* [2001], equatorial region and by *Holfort and Siedler* [2001] and *Saunders and King* [1995], 45°S. The most comprehensive circulation picture probably comes from the global model of *Macdonald* [1998] and the circulation of *Talley* [2003], who manually adjusted Reid's circulation for mass conservation.

[13] The published estimates of meridional overturning circulation consist of 13 to 27 Sv northward flow of thermocline water coming from the South Atlantic that eventually sinks at high latitudes to form the southward flowing North Atlantic Deep Water (NADW) (for a review, see *Talley* [2003]). The NADW flows to the south, mainly in the Deep Western Boundary Current (DWBC) whose transport increases owing to the contribution of Atlantic Antarctic Intermediate Water (AAIW) from above and Antarctic Bottom Water (AABW) from below. The net

NADW export (including the returning AABW) to the Southern Ocean is approximately 20 Sv according to most authors. The AABW is formed in the Weddell Sea and around the continental shelf of Antarctica and flows north in the Atlantic at a rate of about 8 Sv at 30°S, according to current meter measurements [*Hogg et al.*, 1999; *Holfort and Siedler*, 2001]. Part of this flow is entrained into southward flowing NADW within the Brazil Basin; about 2 Sv enters the Guyana Basin [*Hall*, 1997] and 1.2 Sv enters the Eastern Atlantic through the Romanche Fracture Zone [*Mercier and Speer*, 1998].

3.1. Atlantic Setup

[14] At the low-latitude sections 7.5°N and 4.5°S (Figure 2), the temperature and salinity were horizontally filtered in the upper 1000 dbars to decrease the noise in a geostrophic calculation that was enhanced by the small station spacing [*Ganachaud*, 1999]. The part of the North Brazil Current that flows on the continental shelf is added to the transports at 7.5°N with 5 Sv northward [*Johns et al.*, 1998] for mass and 5 Sv times the average tracer concentration in the upper 100 dbars of the western-most 7.5°N station [see also *Lux*, 1997]. A super Tropical Atlantic box was defined between 24°N and 19°S to keep the coupling between the flow north and south of the Equator that is otherwise lost because of the large uncertainties in the equatorial region. Neutral surfaces defining the layers were chosen following previously published works to render comparison easier (Appendix A).

[15] In the original model configuration, the circulation did not conserve mass properly in deep layers and produced systematic negative diffusivities. Because variability in nutrient and oxygen transport is far less quantifiable than variability in mass transports, PO conservation constraints were given lower weights than the original ones in boxes Rio, Tristan da Cunha, and superbox 24°N–19°S so that mass would be properly conserved. The net mass transport across all Atlantic sections was constrained based on the Bering Strait volume and salt transports of *Coachman and Aagaard* [1988] (-0.8 ± 0.6 Sv and 26.7×10^6 kg s^{-1}, respectively). The weight on those constraints also depends on the a priori error budget of Table 2. The Florida Strait transport was constrained to 31 ± 1 Sv [*Schott et al.*, 1988]; the AABW northward flow at 7 ± 2 Sv with 4 ± 0.4 Sv in the Vema Channel [*Hogg et al.*, 1982] and 2.9 ± 1 Sv in the Hunter Channel [*Zenk et al.*, 1999] (at 30°S). Farther North, the AABW transport was constrained at 5.5 ± 2 Sv in the

Table 2. A Priori Uncertainty in the Mass Conservation Equation for a Single Section[a]

Latitudes, °S	Total Flux		Variability of Individual Layers		
	Measurement Noise[b]	Variability	0–1000 dbar	1000–2000 dbar	2000 dbar to Bottom
30	3	6	2	1	0.5
20	5	7	3	2	1
10	10	10	7	3	2
5	20	20	13	7	3

[a]From *Ganachaud et al.* [2000]. The results from the North Atlantic part of the GCM are extrapolated at latitudes less than 20°(S and to the Indian Ocean regions. Values are in sverdrups and represent root mean square quantities.

[b]Measurement noise comes from internal wave activity.
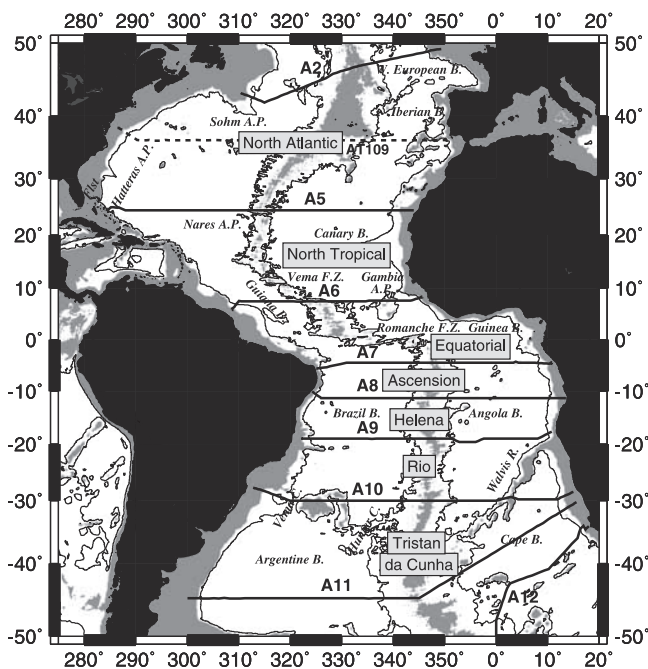
Figure 2. Atlantic Ocean sections and topography. The 4000 m isobath is contoured, and areas shallower than 3000 m are shaded. The light rectangles indicate the box labels. The WOCE sections are A2 (Gauss 226, July 1993) [*Koltermann et al.*, 1999]; A5 (July 1992) [*Parilla et al.*, 1994]; A6 (Feb. 1993) [*Arhan et al.*, 1998] and A7 (Jan. 1993) [*Oudot et al.*, 1998]; A8 (March 1994), A9 (Feb. 1991), and A10 (Dec. 1993) [*Siedler et al.*, 1996]; and A11 (Dec. 1993) [*Saunders and King*, 1995]. At 26°N in the Florida Strait (a continuation of section A5) the 1992 data did not contain nutrients, so that CTD and nutrient data from the 1981 AT109 section of *Roemmich and Wunsch* [1985] were used. The section at 36°N (dashed line) was not used because of biases in the nutrient and oxygen data that were available to me.

western part of the basin at 11°S [*McCartney and Curry*, 1993]; at 3 ± 6 Sv at 4.5°S and at 2 ± 4 Sv at 7.5°N in the western basin [*Hall et al.*, 1997]. There too, the prior uncertainties derive from our error budget. The AABW transport through the Romanche and Chain Fracture zones was constrained at 1.4 ± 3.6 Sv [*Mercier and Speer*, 1998] (the constraint was applied to the zonal transfers between the deep layers of the Equatorial box).

[16] The DWBC was weakly constrained at 20 ± 10 Sv at 7.5°N, according the SOFAR float measurements of [*Richardson and Schmitz*, 1993] (between 900 and 2800 dbars and within 700 km of the coast); at 19°S at −15 ± 7 Sv (1200–2000 dbars); at −11 ± 4 Sv (2000–2800 dbars); and at −13 ± 6 Sv (2800–3600 dbars) according to *Weatherly et al.* [2000]. Reference surfaces are taken from previous works and current meter arrays (Table 3). Integrated mass transports after inversion were insensitive to this choice when compared to the choice of $\gamma^n = 28.11$ as a reference surface. The circulation could accommodate all Atlantic constraints within one standard deviation of the a priori noise range, except for the DWBC transport across 19°S between 2800 and 3000 dbars and the Romanche

Fracture Zone transports. The estimated DWBC transport at 19°S is weaker than by *Weatherly et al.* [2000], probably because of the effect of variability and the limited duration of the measurements. Nevertheless, the values agree within 2 standard deviations. Residual mass imbalances within layers are of O(1 Sv) above 1000 dbars, and very small deeper except for the South Atlantic boxes (19°–45°S) that had higher noise down to 2000 dbars, possibly because of enhanced time variability there. Nevertheless, nowhere are the mass residuals significantly different from zero. The adjustments in the net surface layer transports are smaller than 32% of the initial value (Appendix C, those include any non-geostrophic adjustments, for example, a correction for time variability in the upper layer).

3.2. Atlantic Circulation

[17] From the zonally integrated stream functions (Figure 3), transports in consecutive layers showing the same flow direction are summed (Table 4) to evaluate the main water mass transports. The resulting NADW flow transports 16 ± 2 Sv to the south at 48°N; it aggregates returning AABW and AAIW on its way to the South, for a total transport of −23 ± 3 Sv at 30°S. This result is generally consistent with previous studies, for example, −14 Sv at 48°N; −18 Sv at 24°N [*Wunsch and Grant*, 1982]; 25 Sv at 24°N [*Talley*, 1999, 2003]; 24°N, −20 ± 5 Sv *Roemmich and Wunsch*, 1985]; South Atlantic, −20 Sv [*Fu*, 1986]; −14 Sv between $\gamma^n = 27.5$ and $\gamma^n = 28.11$ at 11°S versus −20 ± 4 Sv here [*Speer et al.*, 1996]; 30°S, −23 Sv [*Holfort and Siedler*, 2001]; and 45°S, −22 Sv [*Saunders and King*, 1995]. The high NADW transport at 24°N of *Talley* [2002] is associated with a 7-Sv northward flow of AABW, which is not reproduced in other estimates. Transports are also consistent with *Macdonald* [1998] almost everywhere, except at 48°N and 11°S where *Macdonald* [1998] obtained larger NADW transports of respectively −26 Sv and −28 ± 1 Sv. The reason for the difference is unclear-possibly time variability [*Koltermann et al.*, 1999] or a problem with the bottom triangle treatment of Macdonald, who used a constant shear below last common depth where we use horizontal extrapolation (*Ganachaud* [2003] found a bias of 30 Sv using Macdonald's method at 48°N). At 4.5°S, our NADW transport is the largest (29 ± 4 Sv). From this same section, *Lux and Mercier* [2001] obtained a similar flow associated with

Table 3. Reference Surfaces in the Atlantic Ocean

Section	Reference Surface	Remark
A2	bottom (LCD)[a]	match to *Clarke et al.* [1998] in the DWBC
Fl. Strait	bottom (LCD)	25 ± 20 cm s^{-1} initial *Schott et al.* [1988, Figure 2]
A5	$\gamma^n = 28.1295$; $\theta \simeq 1.90°$	NADW/AABW
A6	pair-specific	*Lux and Mercier* [2001]
A7	pair-specific	
A8	pair-specific	*Speer et al.* [1996]
A9	pair-specific	*Weatherly et al.* [2000]
A10	$\gamma^n = 28.11$; $\theta \simeq 1.90°$	NADW/AABW
A11	$\gamma^n = 28.11$; $\theta \simeq 1.40°–1.8°$	NADW/AABW - *Saunders and King* [1995]

[a]Last common depth of station pairs.
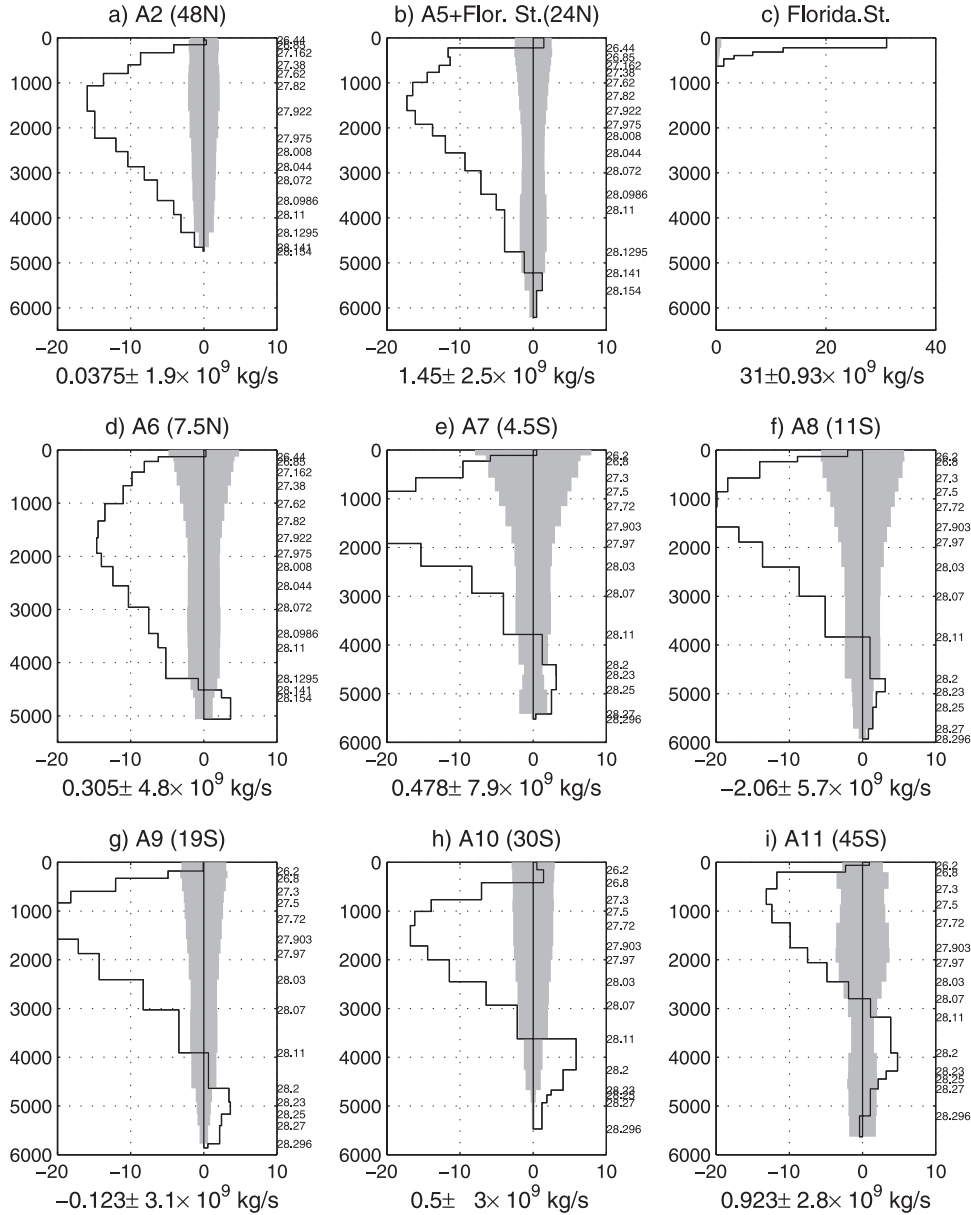
Figure 3. Atlantic Ocean standard circulation. Mass transport across each section is shown, integrated from the bottom (the overturning stream function). The shaded area corresponds to the uncertainty (one standard deviation). The net transport is indicated below each graph; the layer interfaces are indicated on the right of each graph, while depth is an approximate cumulative average pressure. (b) The total transport across 24°N and (c) the transport in the Florida strait alone. Note the different scales on Figure 3c. The net fluxes (numbers below the plots) are indistinguishable from the Bering Strait outflow but are more uncertain because of the baroclinic variability in the upper layers.

large dianeutral transfers between 7.5°N and 4.5°S that accounted for the difference in the overturning structure between the two latitudes. (Noise in the geostrophic transports is largest at those latitudes [*Ganachaud*, 2003]). Within the present error bars, the estimated transports in the North Atlantic are consistent with the *Schmitz and McCartney* [1993, Figure 13] circulation schematic. Comparison is made difficult as *Schmitz and McCartney* [1993] gave no uncertainties. A northward transport of 6 ± 1.3 Sv of Antarctic Bottom Waters is found to enter the Atlantic at 30°S west of the Mid Atlantic Ridge, progressively decreas-

ing to 1 ± 1 Sv at 24°N and 0 Sv at 48°N. In the South Atlantic, the AABW flow is consistent with that suggested by *Hogg* [1999]. However, this circulation conflicts with the description of *Reid* [1994] or *Talley* [2002], of a large production of NADW (29 Sv flowing south at 60°N) that decreases as it flows south.

[18] Net intermediate and surface flows (Table 4, third column, adding Ekman transports) are northward in the range 14–20 Sv outside the equatorial box, becoming consistent with *Macdonald* [1998, Tables 12 and 14], *Schmitz and McCartney* [1993], and *Schmitz* [1996]. Their

Table 4. Atlantic Water Mass Transports[a]

Latitude	AABW	NADW	Intermediate + Thermocline[b]
48°N (A2)	0	−16 ± 2	19 ± 2
24°N (A5)	1 ± 1	−18.5 ± 2	14 ± 2
7.5°N (A6)	3.6 ± 1.2	−18 ± 3	1 ± 4
4.5°S (A7)	3.4 ± 1.2	−29 ± 4	42 ± 7
11°S (A8)	3.1 ± 1.5	−23 ± 4	28 ± 4
19°S (A9)	3.4 ± 1.1	−23 ± 3	26 ± 3
30°S (A10)	6 ± 1.3	−23 ± 3	18 ± 3
45°S (A11)	5 ± 2	−18 ± 4	8 ± 3

[a]Transports (in sverdrups) are summed over consecutive layers of same integrated flow direction (see Figure 3), which does not correspond exactly to the approximate water mass definitions of Tables 8 and 9.
[b]Ekman transport is not included.

vertical structure (Figure 3) indicates a balanced partition between AAIW and surface flow, contrary to the suggestion of *de las Heras and Schlitzer* [1999], of intermediate water flow dominating.

[19] The horizontal structure is presented in the global summary section (Figures 16a–16c) for three global density classes. In the upper layers, large transport variations render arbitrary the definition of boundary currents in many places (Figure 16a). The boundary current transports were determined from stations with common flow direction on the lateral boundaries (Table 5). In the South Atlantic, the present boundary current estimates are in general agreement with estimates from the literature that are based on the same section or on modern current meter arrays, apart from the ambiguity in definition. In the North Atlantic, substantial differences are found, and may be simply due to changes in the circulation. Our boundary current transport uncertainties are underestimated because of unaccounted for baroclinic variability on small scales.

3.3. Dianeutral Transfers and Diffusivity

[20] In bottom layers, upwelling occurs almost everywhere (Figure 4). At deep levels, upwelling dominates in the Equatorial and south subtropical boxes, totaling 5–7 Sv,

depending upon depth. At intermediate levels (1000–1500 dbars), upwelling is found mainly in the Tristan da Cunha (45°–30°S, Figure 4f) box with downwelling found in the Equatorial box, consistent with the NADW southward increase. *Macdonald* [1998] found similar deep upwelling and intermediate downwelling near the equator.

[21] In the North Atlantic and Tristan da Cunha boxes there is downwelling of thermocline waters (−13 ± 3 and −5 ± 2 Sv, respectively), and upwelling in most other boxes. The geostrophic transports in the upper layer combined with horizontal advection across outcropping isopycnals are therefore strong enough to cancel and reverse the convergence of Ekman transports. There is no direct link with the Sverdrup transport though, as our budget includes boundary currents.

[22] Dianeutral diffusivities in the deep layers are mostly positive and systematic over consecutive layers, in the range $0–50$ cm^{2}s^{-1} (Figure 4 (bottom)). The highest diffusivities $(50 ± 50$ cm^{2}s$^{-1})$ are found in the bottom layers where the area of the layer interfaces are small-and subject to uncertainties in their calculation from *Levitus et al.* [1994] and *Levitus and Boyer* [1994]. In the North Tropical, Equatorial, and Rio boxes, diffusivities are significant and in the range $5–20$ cm^{2}s^{-1}. The average diffusivity in the Rio box is of $4.6 ± 3$ cm^{2}s^{-1}, which is similar to the $1–5$ cm^{2}s^{-1} calculated by *Hogg and Owens* [1999]. In the Equatorial and Rio boxes, highest diffusivities are found approximately at the depth of the crest of the Mid-Atlantic Ridge, over which the sharp topography is known to induce enhanced mixing at values reaching 10 cm^{2}s^{-1} [*Polzin et al.*, 1997; *Ledwell et al.*, 2000]. The average diffusivity in the Tropical Atlantic superbox between 24°N and 19°S (see above) below 1000 dbars is $7 ± 2$ cm^{2}s^{-1}(Figure 5), in agreement with *Morris et al.* [2001], who estimated a Brazil basin average at $1–5$ cm^{2}s^{-1} based on a parameterization of bottom roughness. There is no evidence for enhanced dianeutral mixing above 1000 dbars in the Atlantic Ocean; estimates are within the range allowed by the uncertainties-less than $1–2$ cm^{2}s^{-1}, also in qualitative agree-

Table 5. Boundary Currents Estimated From Selected Station Pairs[a]

Latitude	Location	Above γ^n	Name	Estimates, Sv
48°N	50°–43°W	27.82	North Atlantic Drift + recirculations	47 ± 2
				28 [*Macdonald*, 1998]
				37 [*Schmitz and McCartney*, 1993]
24°N	Bahamas-72°W	27.82	upper Antilles Current	27 ± 3
				12 [*Macdonald*, 1998]
				12 [SMC93]
6°N	western end	27.82	North Brazil Current	10[b]
4.5°S	west of 34°W	27.82	North Brazil Current	44 ± 7
11°S	west of 34.7°W	27.5	North Brazil Current	18 ± 4
				40 [*Macdonald*, 1998]
				25 [*Speer et al.*, 1996]
19°S	west of 36.9°W	27.5	Brazil Current (at 23°S)	−15 ± 3
				−13 ± 1 [*Macdonald*, 1998]
30°S	west of 40°W	27.5	Brazil Current	−14 ± 4
				−16 [*Muller et al.*, 1998]
				−22 [*Zemba*, 1991]
30°S	east of 11.8°E	27.5	Benguela Current	14 ± 2
				16 [*Garzoli et al.*, 1996]
			(At 27°S)	23 ± 10 [*Macdonald*, 1998]
45°S	west of 58.4°W	bottom	Falkland Current	30 ± 10
				40 [*Saunders and King*, 1995]

[a]Uncertainties are underestimated as they do not include temporal variability on small scales.
[b]Transport at 6°N changes substantially from one station to the next.
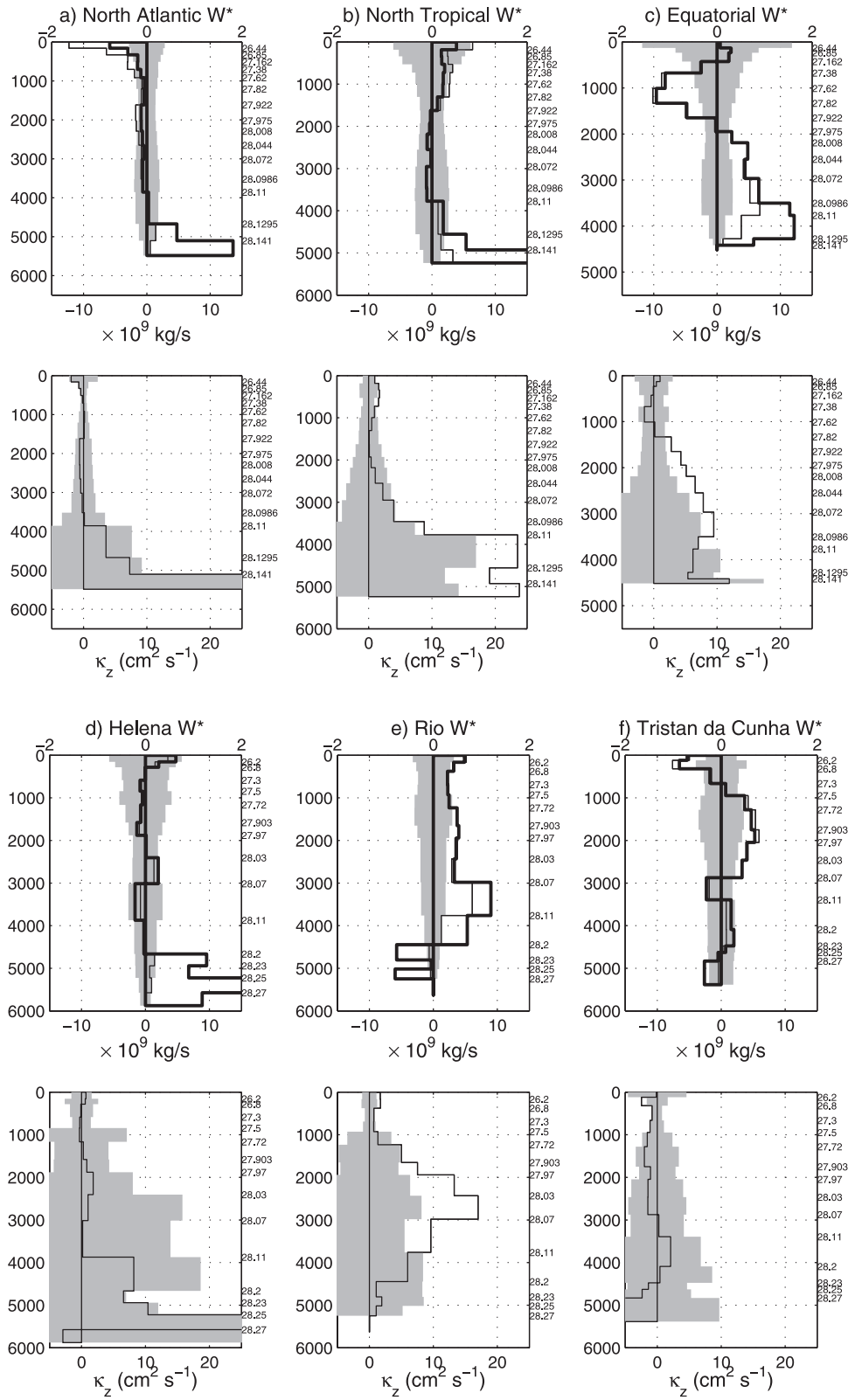
Figure 4. Atlantic Ocean dianeutral transfers. (top) Dianeutral mass transfers (thin line, with the shaded area denoting the one standard deviation uncertainty, and scale given by the lower axis) and corresponding dianeutral velocities (thick line, scale given by the upper axis in units of 10^{-6}m s^{-1}). (bottom) Dianeutral diffusivities. Depth (cumulative average pressure) is given in dbar.
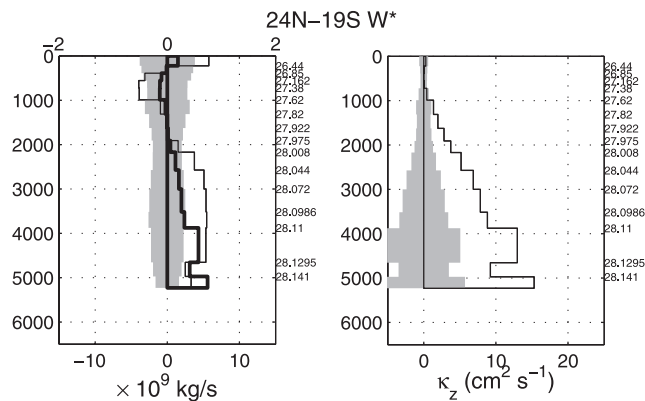
Figure 5. Same as Figure 4 for the central Atlantic box (24°N–19°S).

ment with tracer release experiments that show little mixing near the thermocline [*Ledwell et al.*, 1998]. Basin-averaged diffusivities and dianeutral velocities are discussed in the Summary section.

4. Indian Ocean

[23] The Indian Ocean has a circulation distinct from that of the Pacific or Atlantic ocean because of its strong monsoonal variability (for a review, see *Schott and McCreary* [2001]); its southward average Ekman transport on both sides of the equator; its low-latitude northern boundary; and the net influx of warm water from the Indonesian Throughflow (ITF) (Figure 6). The regional setup and description of our Indian Ocean circulation is given by *Ganachaud et al.* [2000], and we only summarize the main features. Note that the large variability from monsoonal shifts reflects a balance between changes in surface Ekman transports and barotropic return flows [*Lee and Marotzke*, 1998] so that hydrographic measurements are little biased with respect to mean, except near the Somali Current.

[24] At all three latitudes (32°, 20°, and 8°S) we find a deep inflow of 11 ± 4 Sv (Figure 7), similar to that of *Robbins and Toole* [1997] (at 32°S) but with different the zonal and vertical partitions. The weaker deep inflow that is obtained in general circulation models [*Zhang and Marotzke*, 1999] is barely compatible, within an uncertainty of two standard deviations, with these results.

[25] The average ITF is estimated here at 15 ± 5 Sv westward (Figures 7a and 7f), in agreement with recent current meter measurements in the Makassar Strait of 12.5 Sv for a null ENSO index [*Gordon et al.*, 1999] and with the wide range of hydrographic instantaneous estimates (20 Sv westward to 1 Sv eastward) [*Sprintall et al.*, 2002]. However, our estimate is largely dictated by the use of the 1989 JADE cruise, as the adjustments to the thermal wind field are limited by the null flow constraint below sill depth (the 1992 JADE cruise was not used because it contained no nutrient data).

[26] In the Mozambique Channel, there is a southward transport of the same magnitude as the ITF, similar to the Southwest Indian estimate of *Donohue and Toole* [2003]. *DiMarco et al.* [2002] reviewed all existing measurements and model results there and estimated a flow between 6 and 29 Sv southward depending on the section, while *DeRuijter et al.* [2002] found that a train of eddies was transporting an average total of 15 Sv in the channel. Such flow implies a weak or null net flow between Madagascar and Australia (Figures 7d and 7e). At 32°S, the Agulhas Current carries 74 ± 7 Sv to the south, consistently with the previous estimate of *Beal and Bryden* [1997] (69 ± 2 Sv). No obvious horizontal recirculation is observed; the gyre northward wind-driven flow occurs over the whole interior. Underneath, we estimate a northward Agulhas Undercurrent [*Beal and Bryden*, 1997] of 13 ± 5 Sv against the continental slope, with an immediate southward recirculation to its east for an insignificant net transport between the coast of Africa and 35°E in that depth range.

[27] Downwelling is found at the base of the surface layers of the subtropical and North Indian boxes (Figure 8 (top)). Most of the deep upwelling appears to take place in the North Indian box, with about 10 ± 5 Sv. This deep upwelling is returned primarily in the 800–1500 dbars depth range, rather than near-surface. The corresponding "bulk" upwelling velocity ranges from 1 to 3×10^{-5} cm s^{-1} and is associated with bulk dianeutral diffusivities of 4 to 10 cm^2 s^{-1} with larger values in the deepest layer at 30 cm^{2}s^{-1}. In this box, down-gradient mixing is found consistently over all the deep interfaces, with an average diffusivity at interfaces below layer $\gamma^n = 27.36$ and above 28.11 of 8.6 ± 4 cm^2 s^{-1}. Large diffusivities were found in that region (3.5 cm^{2}s^{-1}) [*Johnson et al.*, 1998], possibly because of the rough North Indian Ocean topography.

5. Pacific Ocean

[28] In the South Pacific, previous regional estimates of the deep water northward flow range 11 to 20 Sv, the main ones being from *Warren* [1973] (DWBC from the Scorpio sections of *Stommel et al.* [1973]); *Wunsch et al.* [1983] (12 Sv, same data); *Tsimplis et al.* [1998] (12 Sv from the WOCE data); *Wijffels et al.* [2001] (16 to 20 Sv from WOCE including floats); *Roemmich et al.* [1996] (11 to 14 Sv from current meter and hydrographic measurements at 10°S); *Whitworth et al.* [1999] (15 Sv from current meter measurements in the western Southwest Pacific basin at 32°S with a ±10 Sv variability); and a review by *Talley and Roemmich* [1991]. The global model of *Macdonald* [1998] yielded a more moderate bottom water inflow of 8 ± 5 Sv at 43°S from the older Scorpio data.

[29] In the North the estimated deep inflow at 10°N ranges from 9.6 Sv [*Johnson and Toole*, 1993] to 8 Sv [*Wijffels et al.*, 1996]. North of 24°N, *Roemmich and McCallister* [1989] (hereinafter referred to as RMC89) used an inverse model combining zonal and meridional sections to estimate a 10 Sv deep inflow at 24°N and 0.7 Sv to the north across 48°N. In this same region, the *Macdonald* [1998] model also suggested a weaker bottom water flux of 5 ± 3 Sv at 24°N, although it could be consistently constrained at a 10 Sv flow. As will be seen in our inverse model, a significant northward bottom water flow at 24°N is incompatible with conservation of heat and salt in the North Pacific.

5.1. Pacific Ocean Setup

[30] A gap of a few stations in the phosphate data set in P6 (32°S) was filled with a local nitrate-phosphate Red-
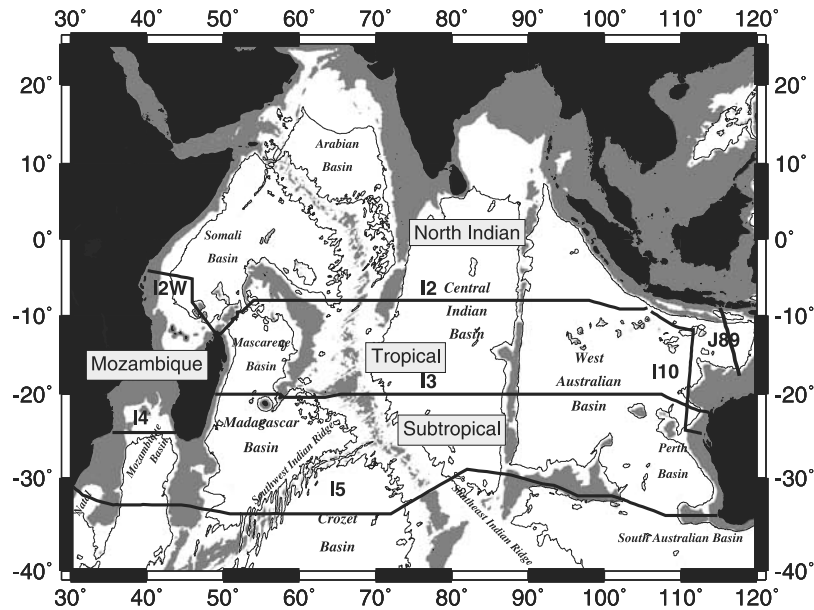
Figure 6. Indian Ocean sections and topography. The data set is made of the WOCE sections I2 (Dec. 1995 to Jan. 1996 [e.g., *Johnson et al.*, 1998]); I3 (April–June 1995); I4 (June 1995); I10 (Nov.–Dec. 1995 [*Bray et al.*, 1997]); the pre-WOCE section I5 (Nov. 1987 [*Toole and Warren*, 1993; *Robbins and Toole*, 1997]); and the Java Australia Dynamics Experiment (JADE) section (Aug. 1989 [*Fieux et al.*, 1994; *Coatanoan et al.*, 1999]). (The 1989 JADE data were used instead of the 1992 data because they included nutrient measurements. However, the 1989 data were combined with a station of the 1992 data to complete the section. Reproduced from *Ganachaud et al.* [2000].)
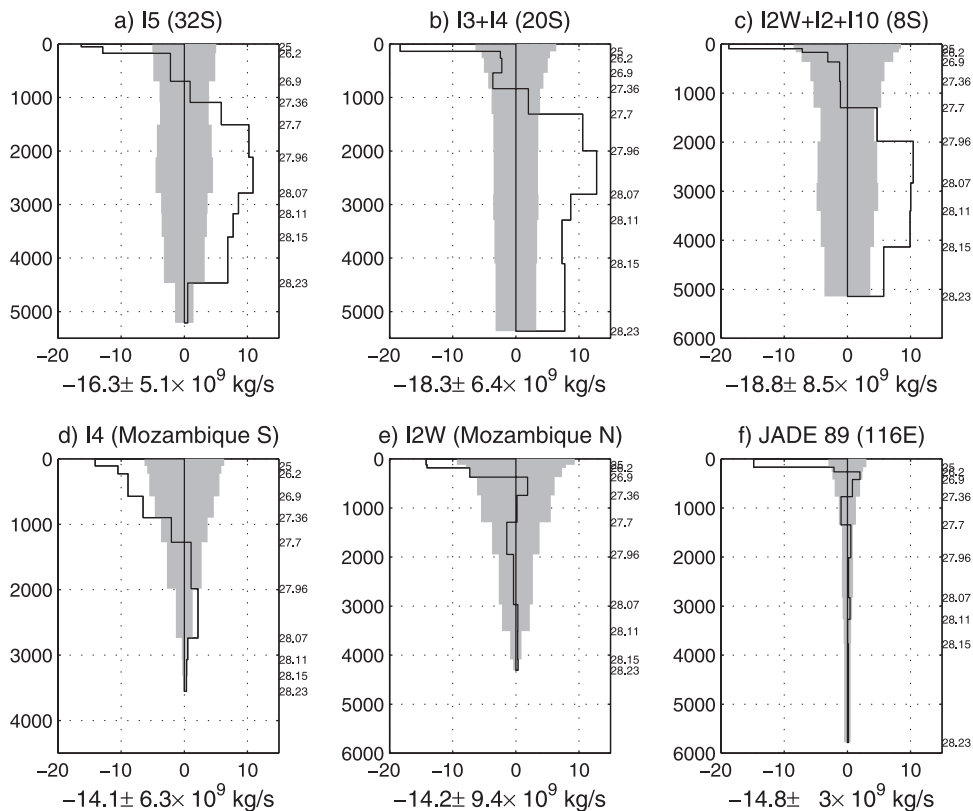
Figure 7. Indian Ocean standard circulation across latitudes (a) 32°S; (b) 20°S; (c)8°S; (d) across the southern and (e) northern Mozambique Channel; and (f) across the PIT. (Same as Figure 3; from *Ganachaud et al.* [2000]).
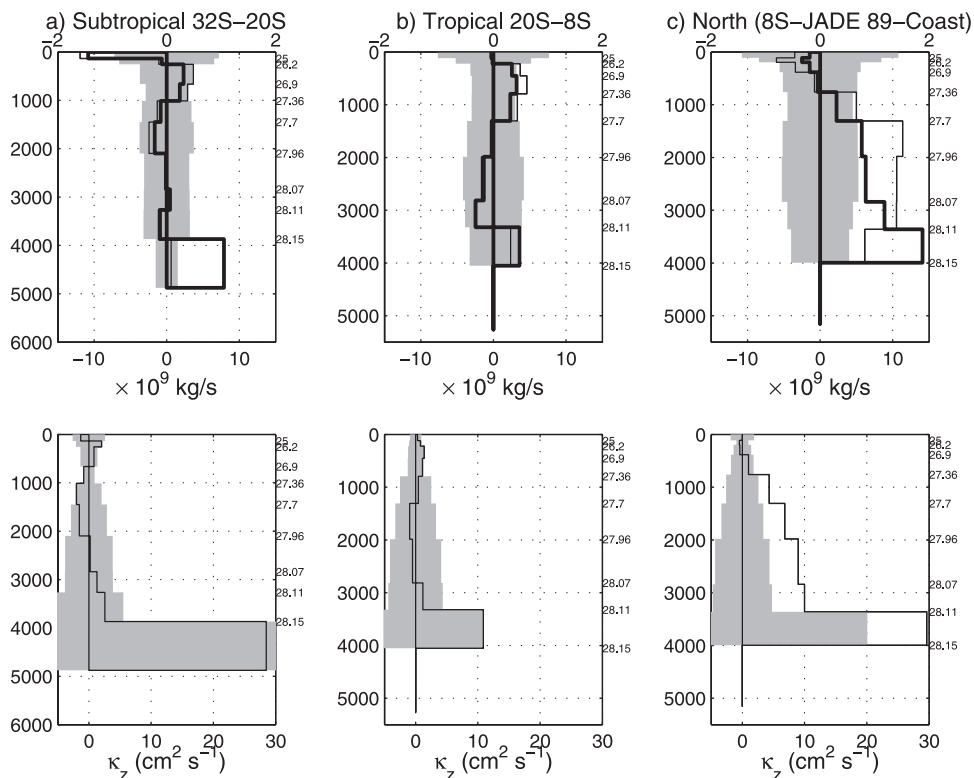
Figure 8. Standard solution dianeutral mass transfers and diffusivities for the (a) subtropical, (b) tropical, and (c) north regions in the Indian Ocean. (Same as Figure 4; from *Ganachaud et al.* [2000].)

field relation. Conservation was required in deep layers of the Aleutian box (Figure 9) as water properties suggest no deep water formation in the North Pacific [*Warren*, 1983], the deepest winter convection affecting layers above 1000 dbars at 47°N [e.g., *Reid*, 1965, pp. 50–51]. (CFC measurements suggest that some bottom water was formed during the past 40 years in the Bering Sea, but in very small amounts [*Warner and Roden*, 1995].) The net northward flux across 32°S and 17°S was constrained at the a priori Bering strait+ITF transport, 7.8 ± 10 Sv [*Ganachaud et al.*, 2000]. At 32°S between 179°W and 168°W the deep water transport was constrained at 16 ± 5 Sv northward below $\gamma^n = 27.95$ ($\theta = 1.75°$ according to *Whitworth et al.* [1999] (hereinafter referred to as WWNRPM99). The ±5 Sv uncertainty is their estimated variability in the baroclinic transport from repeat sections, which is half the total variability as measured from the current meters. Importantly, the authors found that the P6 baroclinic transport was representative of the average of 3 repeat sections. The vertical structure of that transport was constrained according to WWNRPM99 [see *Ganachaud*, 1999]. The deep flow through 17°S was constrained at 12 ± 4 Sv below $\gamma^n = 27.95$ in the Samoa Passage region [*Roemmich et al.*, 1996]. (The *Roemmich et al.* [1996] estimate is for the total northward transport below $\theta = 1.2°C$ at 10°S, while WWNRPM99 estimated only the western contribution.) The deep flow was also constrained according to bathymetry (Appendix B, Table B2). Reference surfaces were chosen at the top of the northward flowing Circumpolar Deep Water (Table 6). An experiment with the 17°S reference surface moved to $\gamma^n =$

27.95 ($\theta \simeq 2°$) led to similar integrated mass transports after inversion.

[31] Almost all constraints were met within their a priori range. The WWNRPM99 constraint of net flow of 16 ± 5 Sv was met as 11 ± 3 Sv; however, the vertical partition suggested by WWNRPM99 could not be reproduced within one standard deviation of the constraint: the model produced northward transport higher than the ones prescribed below 4250 dbars with 10 ± 2 Sv and lower just above with 4 ± 1 Sv. Residual layer mass imbalances are smaller than 0.5 Sv and indistinguishable from zero within two standard deviations.

5.2. Pacific Circulation

[32] Across 32° and 17°S there is a net northward transport of 16 ± 5 Sv (values below Figures 10a and 10b). The net flow between New Caledonia and Australia is uncertain and to the south, −8 ± 11 Sv (Figure 10c), implying a 24 ± 12 Sv northward transport between New Caledonia and Peru, similar to the transports of *Tsimplis et al.* [1998]. At 32°S in the Tasman Sea, the total transport between Australia and 170°E is also southward, with −10 Sv.

[33] In the South Pacific, net northward flow of deep water is found at approximately 8 Sv (Figures 10a and 10b). At 32°S, most of that flow occurs in the bottom layer below $\gamma^n = 28.18$ ($\theta \simeq 0.8°$) at 8 ± 2 Sv, while at 17°S the bulk of the northward flow occurs higher in the water column, with 7 ± 1.3 Sv below $\gamma^n = 28.1$ ($\theta \simeq 1.2°$). Dianeutral transfers account for this shift. The DWBC against the Tonga-Kermadec ridge at 32°S has a strength
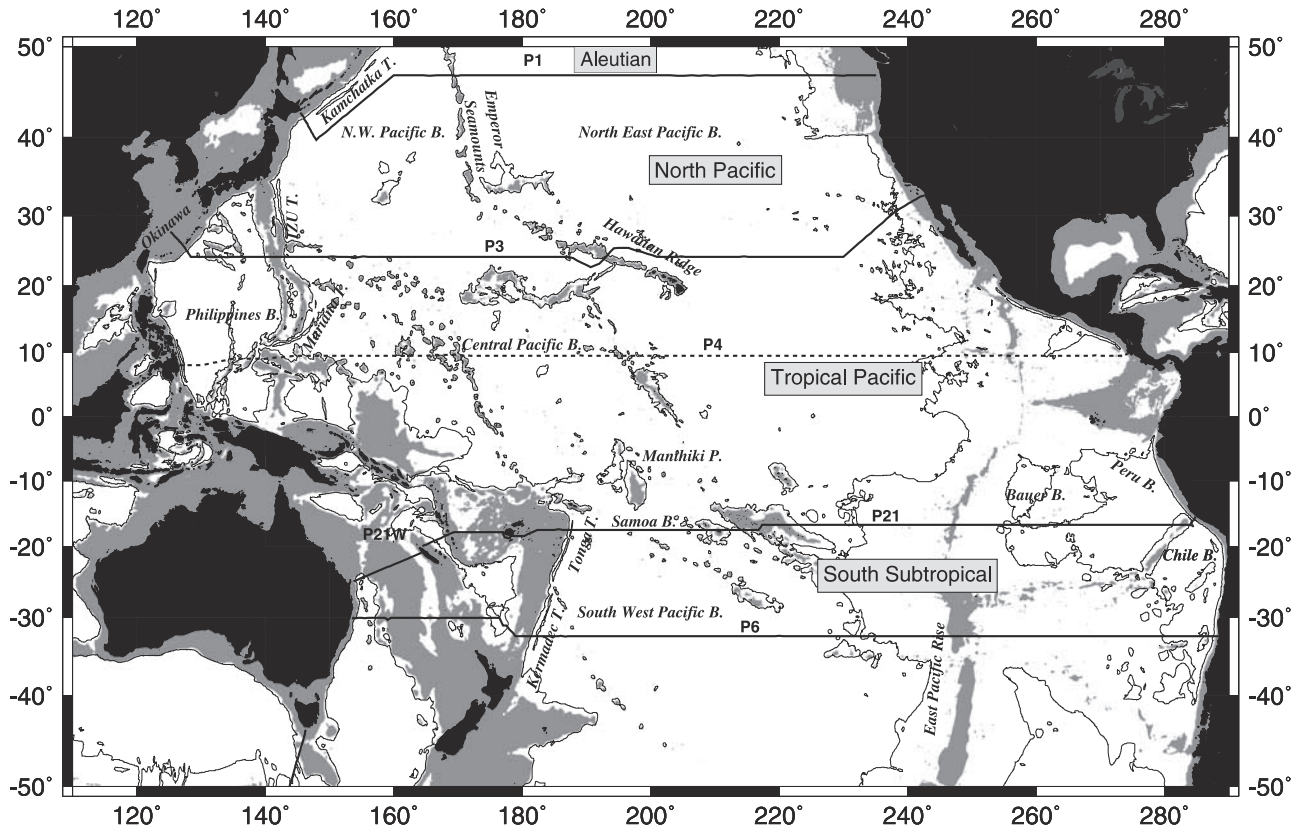
Figure 9. Pacific Ocean sector of the model is made of the pre-WOCE sections P1 (Aug. 1985) and P3 (April–May 1985) and the WOCE sections P21 (April–June 1994) and P6 (May–July 1992). An attempt to use P4 (10°N, Feb.–May 1989) gave rise to large downward mass transfers at intermediate levels, probably because of the baroclinic variability in the Mindanao Current (S. Wijffels, personal communication, 1998), which made the section incompatible with the rest of the circulation. It was thus decided not to use P4 (dashed line) in the present model. I chose not to use the WOCE line P2 at 30°N (Bando, Fukasawa, and Okuda; Nov.–Feb. 1994) because of the large time offset from the surrounding sections P3 and P1. The 4000 m isobath is contoured, and areas shallower than 3000 m are shaded.

of 17 ± 3 Sv below $\gamma^n = 27.95$ ($\theta \simeq 1.9°$). With no PO conservation constraint, the deep inflow is of 15 ± 3 Sv and associated with larger mass imbalances at intermediate and deep levels in the tropical Pacific. This solution is physically acceptable as well. It hardly overlaps with the standard one, suggesting that the a priori weights on some of the constraints may be too high. For instance, there is a trade-off between the WWNRPM99 constraint, the PO constraint, and residual mass imbalances in the tropical Pacific. While the 22 months time series of WWNRPM99 may be too short to estimate a mean flow, the weight on the PO constraints were chosen somehow arbitrarily [*Ganachaud et al.*, 2000, Appendix A]. The solution of low overturning was retained because of the smaller mass residuals.

[34] In the North Pacific at 24°N (Figure 10d) the deep inflow is indistinguishable from zero in the bottom layers below $\gamma^n = 28.09$ ($\theta \simeq 1.15°$). Still, there is a substantial amount of northward flowing deep water ventilating the basin (Figure 16c) but this same amount returns south in the same density range. Most published estimates are in the range of $10-13$ Sv from regional analyses and of 5 to 8 Sv from the global [*Macdonald*, 1998] model. The flow of *Talley* [2003] suggests 3 Sv Circumpolar Deep Water

(CDW) (CDW = NADW + AABW mixture) going North and 6 Sv PDW going south just above. The RMC89 circulation (10 Sv inflow) conserved mass only top-to-bottom: no conservation statements were applied in individual layers. (They used the same 24° and 47°N sections as ours combined with one at 36°N and several meridional sections.) This inflow requires 60 cm^2s^{-1} diapycnal diffusivities to the north-a large value for the North Pacific where

Table 6. Reference Surfaces in the Pacific Ocean

Section	Reference $\gamma^n(\theta)$	Remark
P6	28.10(1.1)	. . .[a]
P21	28.10(1.3)	. . .[b]
P3	27.95(1.6)	2000 dbars [RMC89]
P1	28.09(1.1)	4000 dbars [RMC89]

[a]At 32°S, near the deep western boundary current against the slope of the Kermadec ridge, the current meter results of WWNRPM99 showed that the limit of the northward flowing waters did not coincide with any water mass boundary as classically used as reference surfaces The initial velocity field was thus adjusted to match their 2-year mean absolute velocity.

[b]At 17°S against the Tonga Ridge, the reference surface was moved just above the high shear region of the deep western boundary current Away from the boundary currents, the reference was taken at $\theta = 1.1°$ or 1.3° [*Banks et al.*, 1995; *Tsimplis et al.*, 1998].
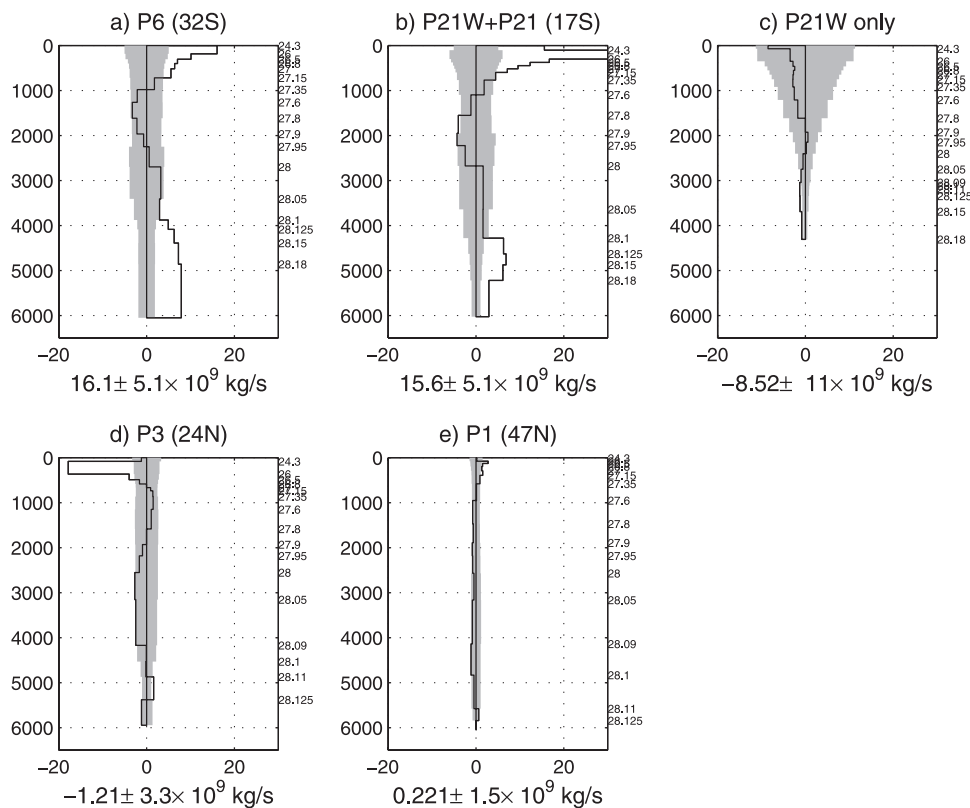
Figure 10. Pacific Ocean standard circulation. (Same as Figure 3.) (b) The total transport across 17°S and (c) the transport between New Caledonia and Australia only (P21W).

topography is smooth [see, e.g., *Morris et al.*, 2001]. In our case, the deep inflow is determined by salt anomaly conservation in the North Pacific deep layers. An experiment without salt conservation produced a 5 Sv deep inflow with strong upwelling ($w* \simeq 4 \times 10^{-5}$ cm s^{-1}, see section 7 for $w*$ values) and vertical mixing (60 cm^{2}s^{-1}) at 4000 dbars between 24° and 47°N. A deep reference surface choice ($\gamma^n = 28.11$, the upper limit of the deep inflow of RMC89) did not cause substantial changes; neither did a 10 ± 5 Sv constraint on the deep inflow. The RMC89 circulation in the North Pacific could be reproduced by suppressing conservation in individual layers. The *Macdonald* [1998] circulation (an inflow of 5 ± 3 Sv at 24°N) imposed no heat conservation and a lower weight on salt conservation because the anomaly formulation was not used. It is not clear whether our low inflow is an actual feature or whether it is model-dependent, for instance, because of our limited representation of vertical exchanges.

[35] Just above the northward flowing bottom waters, the deep flow (2000–4000 dbars) is directed southward in the South Pacific. Most of it occurs between 170°W and 140°W at 32°S (Figure 16b), greatly contrasting with the speculative interior circulation that WWNRPM99 inferred from a [*Stommel and Arons*, 1960] schematic combined with the current meter measurements. The northward bottom inflow topped by southward mid-depth return flow is similar to that of *Wunsch et al.* [1983], *Macdonald* [1998], and *Wijffels et al.* [2001]. The bulk of the bottom water flow occurs below $\gamma^n = 28.19$ ($\sigma_4 = 45.96$, about 4500 m on average, 4100 m in the DWBC and 5400 m at 150°E) by *Wunsch et al.*

[1983] (note that the pressure scale is distorted), as well as here. *Macdonald* [1998] and *Wijffels et al.* [2001] would suggest that the northward net inflow occurs monotonically from the bottom all the way up to 4200 m. (Comparison is uncertain because of the different coordinate systems.) At 17°S, our estimated bottom inflow occurs in density layers up to $\gamma^n = 28.1$ (3800 dbars).

[36] At 30°S, examining the upper layers, the East Australian Current (EAC) closes the subtropical gyre with a strength of 36 ± 10 Sv southward (Figure 16a Australia to 154.5°E; surface to $\gamma^n = 27.95$), similar to *Macdonald* [1998, p. 348] and *Chiswell et al.* [1997]. At 25°S, the estimated EAC strength is somewhat smaller at 25 ± 6 Sv southward (Australia to 155°E). Both estimates are consistent with those of *Tsimplis et al.* [1998]. At both latitudes, an immediate recirculation returns about 80% of the EAC to the north within 500 km of the current. The Peru-Chile Current on the eastern side of P6 carries 8.5 ± 4 Sv to the north at 30°S (surface to $\gamma^n = 27.95$; 75°W to Peru). At 16°S (P21E), the flow is to the south against the coast (-8 ± 2 Sv), with a 22 ± 2 Sv northward jet offshore and eddy-like motion farther west.

[37] In the North Pacific, the subtropical gyre at 24°N is closed by the Kuroshio (Figure 16a, 68 ± 7 Sv to the north between the surface and $\gamma^n = 27.95$ and from the western boundary to 130°E), similar to *Macdonald* [1998] or *Worthington and Kawai* [1972, p. 373] (60 Sv). About 2/3 of this flow is returned south between 132° and 134°E and 1/3 over the rest of the basin. The Kuroshio transport in the East China Sea alone is 28 ± 6 Sv, similar to that of *Macdonald*
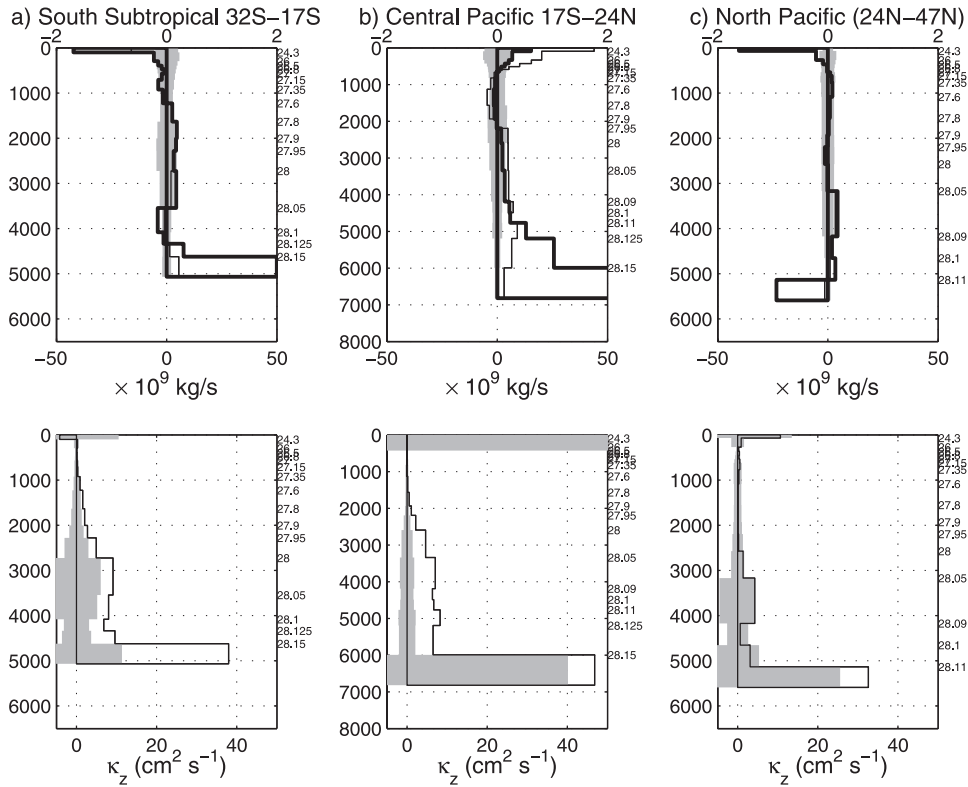
Figure 11. Dianeutral transfers and diffusivities in the Pacific Ocean. (Same as Figure 4.)
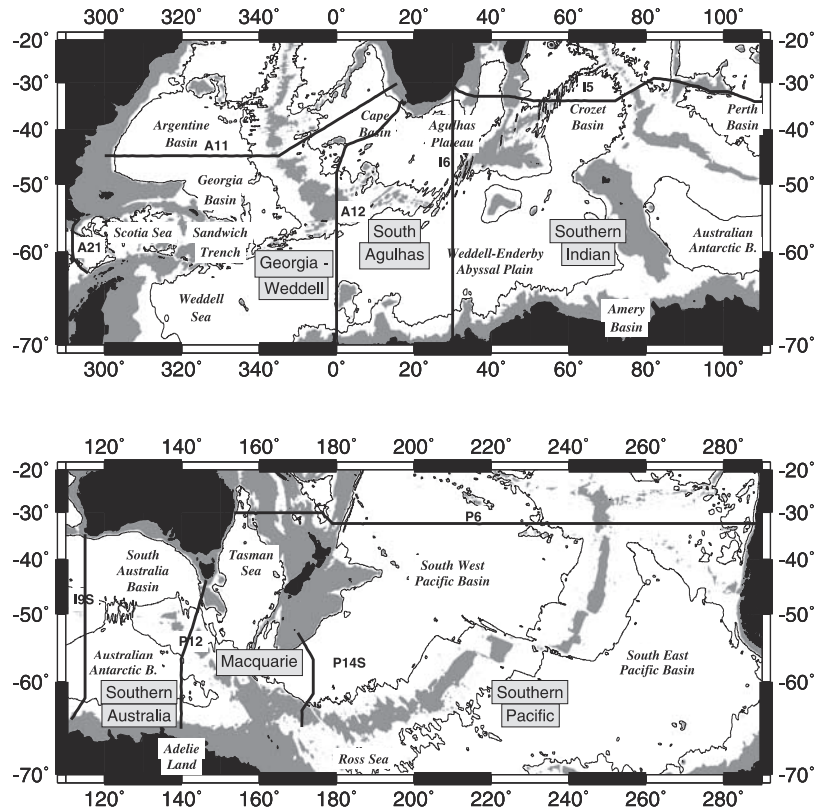
Figure 12. Southern Ocean meridional lines: A21 (Drake, Jan. 1990 [*Roether et al.*, 1993]); A12 (May 1992 [*Lemke*, 1994]); I6 (Feb. 1996 [*Park et al.*, 2001]); I9S (Dec. 1994 [*Hufford et al.*, 1997]); P12 (Jan. 1995 [*Rosenberg et al.*, 1997]) and P14S (Jan. 1996 [*McTaggart and Johnson*, 1997]). The 4000 m isobath is contoured, and areas shallower than 3000 m are shaded.
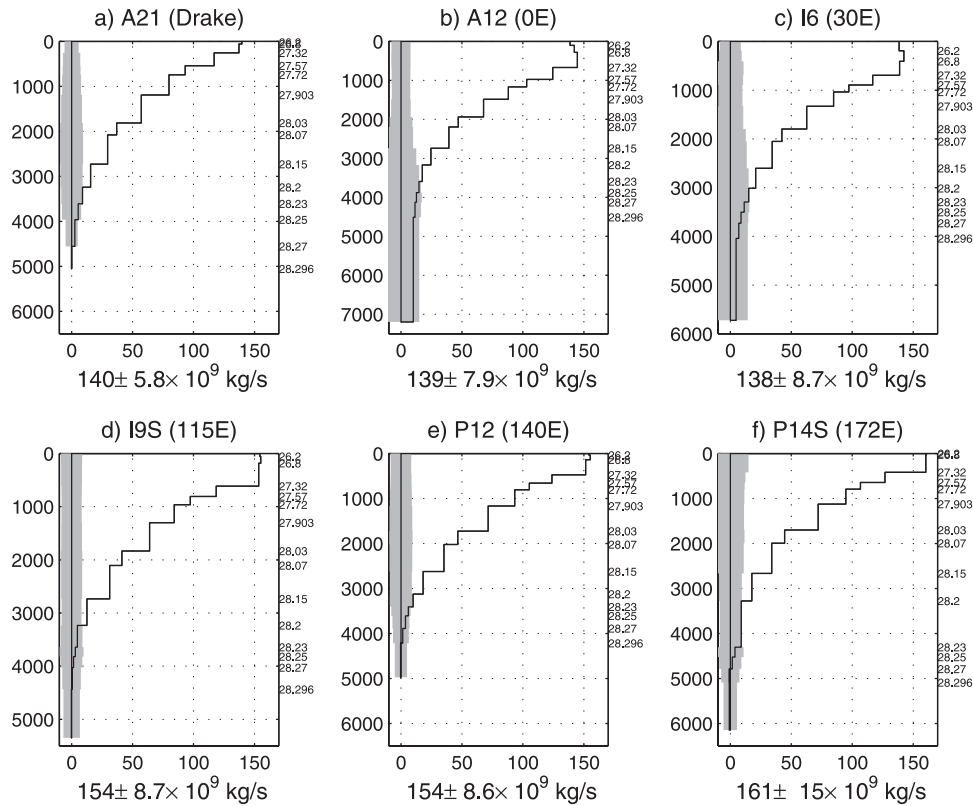
Figure 13. Southern Ocean standard circulation (same as Figure 3). The meridional slope of the layers are steep (all layers outcrop), and the depth on the graph indicates the cumulated average thickness of the layers.

[1998] and RMC89 but is nevertheless higher than recent current meter observations 400 km upstream of 22 ± 2.5 Sv [*Zhang et al.*, 2001], possibly because of interannual variability [*Ichikawa and Beardsley*, 1993], or to a mass influx through the Ryukyu Islands. At 47°N, a northward flow is found close to the coast (31 ± 7 Sv from the surface and $\gamma^n = 27.95$ and west of 146.5°E), probably because of a warm eddy emanating from the Kuroshio Front [*Kawai*, 1972, p. 248]. Farther east, the Oyashio carries 37 ± 2 Sv (146.5°E to 148.4°E) south.

5.3. Dianeutral Transfers and Diffusivity

[38] Upwelling is found at the surface in the Tropical Pacific (Figure 11b, 45 ± 6 Sv), similar to the values for Equatorial upwelling estimated from drifters and hydrographic measurements (50 Sv and 62 ± 18 Sv, respectively) [*Johnson*, 2001; *Johnson et al.*, 2001]. Downwelling is found in the subtropical gyres (-16 ± 5 Sv in the South Pacific; -17 ± 3 Sv in the North Pacific) (Figures 11a and 11c). At depth, and in the South and tropical Pacific, there is upwelling below 2000 dbars associated with systematic and significant diffusivities ranging from 1 to 8 ± 2 cm^2 s^{-1} between 2000 and 4500 dbars (Figures 11a and 11b). Diffusivities across the deepest layer interface are larger at about 40 cm^{2}s^{-1}. An approximate heat balance by *Roemmich et al.* [1996] already suggested dianeutral diffusivities of 60 to 1000 cm^{2}s^{-1} downstream from the Samoan Passage. In the deep North Pacific, dianeutral diffusivities are positive, but not significant.

[39] The magnitudes of the vertical transfers and diffusivities are similar to the ones of *Macdonald* [1998] and *Wijffels* [1993]. In the South Pacific, *Tsimplis et al.* [1998] obtained a smaller upwelling of a few tenths of a sverdrup below 3500 dbars and downwelling above 3500 dbars. *Macdonald* [1998] obtained no significant vertical exchanges there. On the other hand, she estimated significant upwelling in the North Pacific which we do not because of the weaker deep inflow discussed above.

6. Southern Ocean and Bottom Water Formation

[40] Contact with the atmosphere or sea ice permits formation of the dense AABW along the shelf of Antarctica. As a result, all of our layer interfaces above 4000 dbars north of 30°S reach the surface in the Southern Ocean, in our data set. The Weddell Sea has been in the past regarded as the main formation site but recent observations indicate other formation regions such as the Amery Basin, Adélie Land, the Ross Sea, and the western Weddell Sea (Figure 12) [*Rintoul*, 1998; *Orsi et al.*, 1999; *Sloyan and Rintoul*, 2001]. The total amount of AABW being produced is not well agreed upon yet. *Mensch et al.* [1996] estimated a minimum of 14 Sv of AABW production around Antarctica from CFC data and a water mass box model. However, *Broecker et al.* [1999] suggested a dramatic reduction over the past 800 years from 15 to 5 Sv in the Southern Ocean bottom water formation based on estimates from CFC, PO$_4^*$ and ^{14}C and mixing lines. Their speculative results were contradicted by *Orsi et*
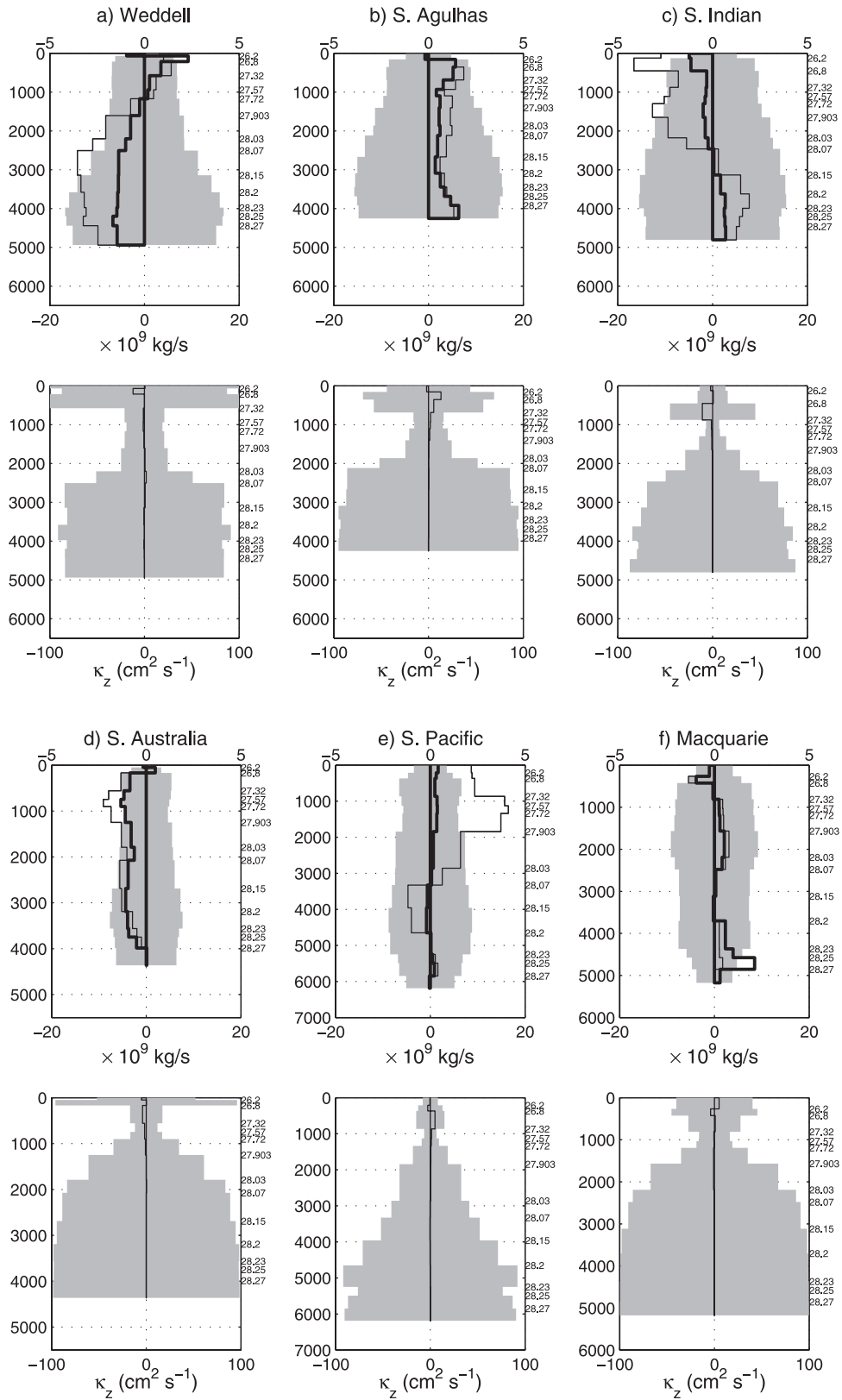
Figure 14. Dianeutral transfers and diffusivities in the Southern Ocean. Again, layer depth is an average cumulative pressure as all layers outcrop. (Same as Figure 4.)
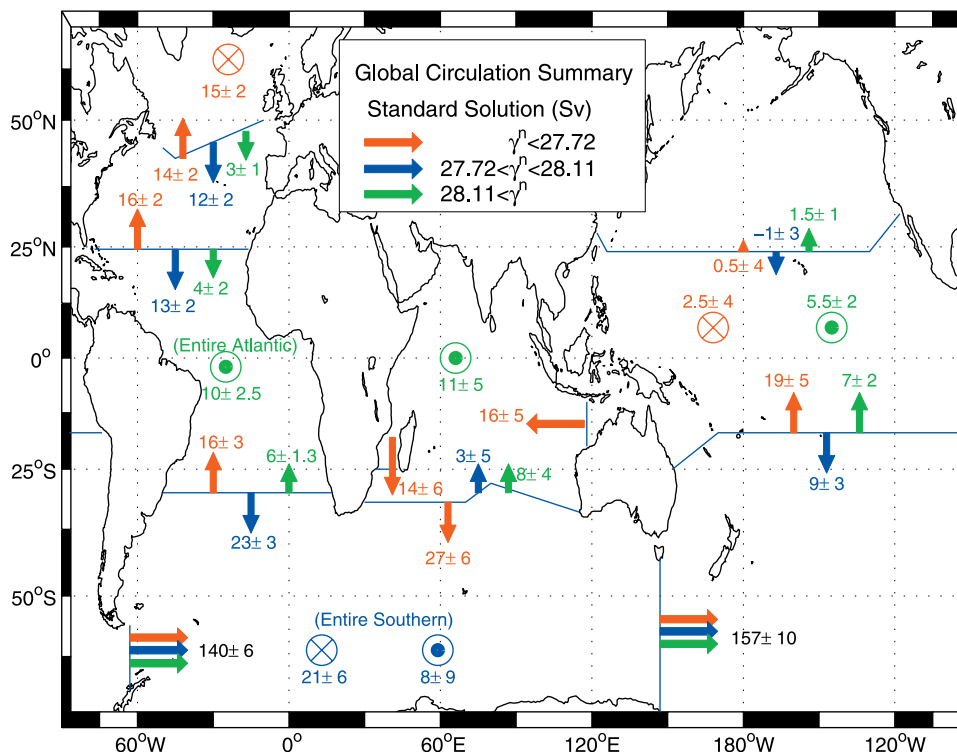
Figure 15. Zonally integrated layer mass transports. The estimated water transports are indicated for the different density classes bounded by neutral surfaces (γ^n, in kg/m^3) and across selected hydrographic sections. The color of the upwelling or downwelling arrows indicates the layer from which the water is coming. Actual numbers are rounded off (within uncertainties) so that total transports are mass conserving. In the Southern Ocean the bottom water formation takes place mostly in the Weddell Sea, while the upwelling distribution is uncertain. In the Indian ocean most of the upwelling takes place north of 7°S. The South Pacific transports are given at 17°S because of the more complicated structure at 32°S (section 5). From *Ganachaud and Wunsch* [2000].

al. [2001], who argued that the comparison was wrong and, dividing the abyssal ocean in two density classes, reconciled the CFC and the ^{14}C estimates. All regional estimates based on hydrographic sections suggest deep water production similar to that of *Mensch et al.* [1996] with 15 Sv or more in the Southern Ocean, with an extreme at 50 Sv [*Sloyan and Rintoul*, 2000].

6.1. Southern Ocean Setup

[41] A box between P12, P14S and the western part of P6 was defined (Macquarie Box), in addition to the main Pacific boxes of Figure 12, with weaker conservation constraints because P14S did not reach the Antarctic continent and the box was not closed between P6 and New Zealand down to 2000 dbars. An additional super box was defined in the Southern Indian between A12-I5-I9S. The neutral surfaces defining water masses are given in Appendix A. Because of the possible atmospheric exchanges at the outcrop, conservation of heat and PO was not required and the a priori noise in the salt anomaly equations was increased to $\pm(35$ g/kg$) \times (1$ Sv$)$ to account for freshwater exchanges. Thus only mass and total silica had an effective influence so that dianeutral transfers and diffusivities are essentially determined by constraints from outside the Southern Ocean.

[42] The net transport through Drake Passage was constrained at 140 ± 6 Sv eastward, according to current meter

and hydrographic transport estimates [*Whitworth et al.*, 1982]. (140 ± 5 Sv is the weighted average of their estimates with respective uncertainties as by *Macdonald* [1995]; increased by 1 Sv RMS from our error budget.) All reference surfaces were taken at the bottom (last common depths of station pairs) where velocities are likely to be the weakest. A large range is allowed in the dianeutral transfers ($\pm 10^{-3}$ cm s^{-1} and ± 100 cm^{2}s^{-1}) because little is known about water formation and also because the advection-diffusion formalism may be inappropriate there [*Sloyan and Rintoul*, 2000].

[43] All constraints were formally met. Mass imbalances in the Macquarie box indicated a systematic, but non-significant convergence (-5 ± 7 Sv), possibly because of unaccounted flow South or North of New Zealand. (The section does not reach Antarctica, but the Ross Sea Gyre south of P14S generally flows westward.) Because wind is nearly perpendicular to the sections, the zonal Ekman transports are weak (Appendix C).

6.2. Southern Ocean Circulation

[44] The Drake Passage flow is found close to its constrained value with 140 ± 6 Sv (Figure 13). South of Australia, the net transport is increased by the Pacific-Indonesian Throughflow with 154 ± 9 Sv, which is similar to the regional calculation of *Rintoul and Bullister* [1999]. Generally the transports increase almost linearly above 3000
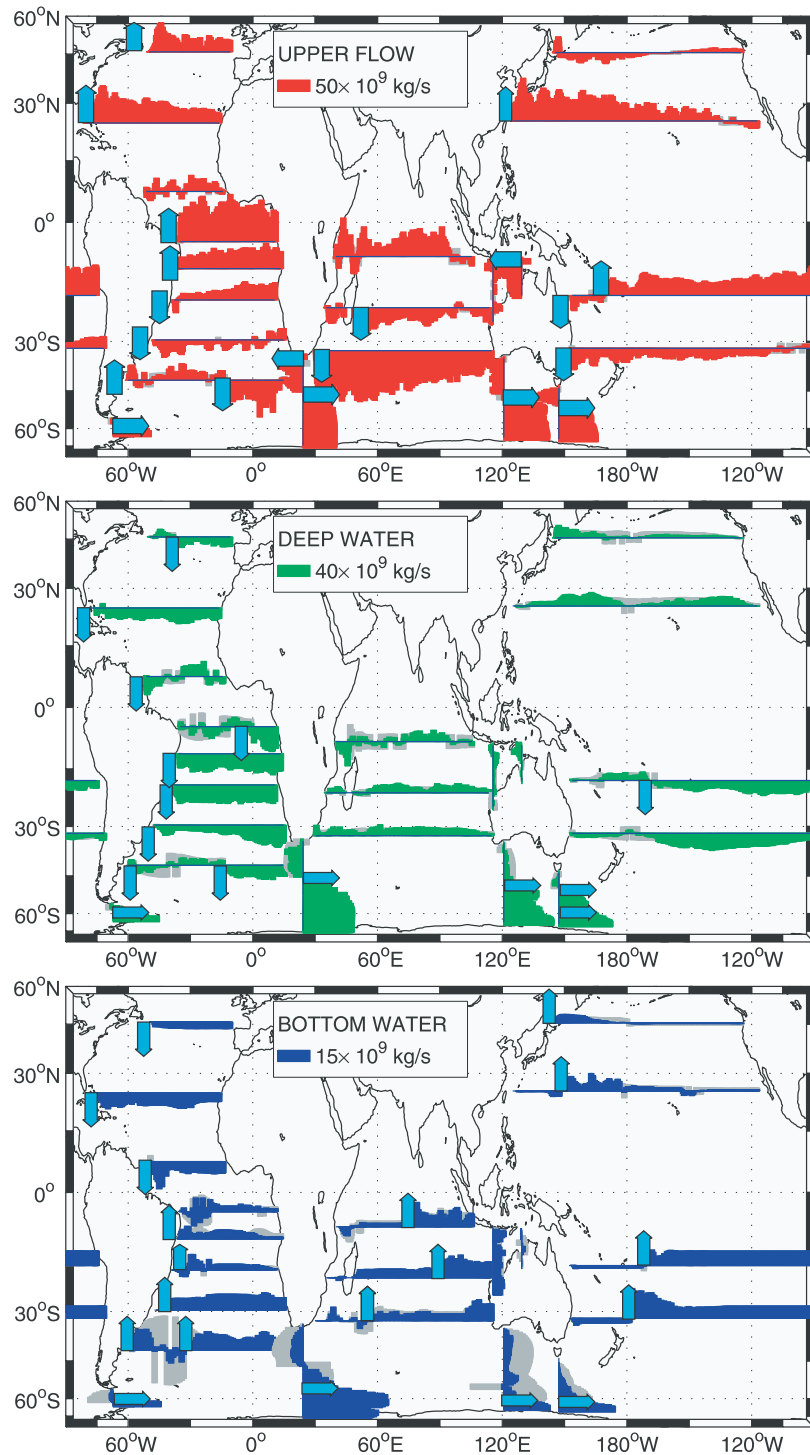
Figure 16. Horizontal partition of the flow for the layers of Figure 15. The full color shows the transport integrated cumulatively from west (north). The light shaded areas are for the corresponding one standard deviation uncertainty. The main strong currents are indicated by the arrows. Section position are approximative for clarity. South of Africa, only A12 is plotted. Small sign changes in cumulative transports trigger spikes in the shaded bars (i.e., Atlantic, 45°S).

dbars giving a parabolic shape to the stream function. The latitude of the ACC maximum shifts southward as density increases (Figures 16a–16c.)

[45] In the Weddell sea where the first six layers outcrop north of the ACC, there is an uncertain mass transfer from dense to light water near the surface (6 ± 7 Sv, Figure 14a). Similar buoyancy gains are observed in the Agulhas box (Figure 14b) and in the Southern Pacific (Figure 14e, 13 ± 5 Sv). In contrast, in the Southern Indian and Southern Australia regions there is buoyancy loss (Figures 14c and

14d) so that the resulting net water mass transformation through γ^n = 27.72 (CDW, with same density as the upper NADW in the South Atlantic) is uncertain at 6 ± 9 Sv. Conversion of CDW into AAIW has been suggested from observation [*Schmitz and McCartney*, 1993] and numerical simulations [*Shriver and Hurlburt*, 1997] but neither *Macdonald* [1998] and *Sloyan and Rintoul* [2000] nor *Talley* [2003] displayed density loss at this interface.

[46] Deep and bottom water formation is inferred in the Weddell Sea with −14 ± 11 Sv crossing γ^n = 28.15, consistent with the *Rintoul* [1991] AABW production estimate at 9 Sv. Deep transfers are uncertain in all other boxes but because uncertainties are correlated, the total southern deep water formation across γ^n = 28.15 is significant at −20 ± 6 Sv. While *Macdonald* [1998] did not quantify the bottom water formation rate, *Sloyan and Rintoul* [2001] obtained a comparable value across γ^n = 28.20. However, just above-across γ^n = 28.0, their water mass transfer was much larger at 50 Sv, implying a much larger deep inflow into the Pacific and Indian basins than the one that is permitted by the present model (sections 4 and 5). Their different treatment of dianeutral exchanges as independent values for each property may allow an artificially high estimate, and is I believe unrealistic in the deep ocean except in water mass transformation regions such as the Southern Ocean. *Sloyan and Rintoul* [2000] determined their initial water mass transfers from the meridional Ekman transport of whereas we have null initial transfers and allow a large range of adjustment to the dianeutral transfers (w^* = ±10^{-3} cm s^{-1}). We use this approach because it is not clear how the Ekman transport and other oceanic processes interact to produce the water mass conversion. Such a large range of adjustment makes the result insensitive to the prior choice of w^*, but at the expense of increasing the final error bar.

[47] Our estimate of Southern Ocean bottom water formation is therefore in agreement with most previous estimates-given the large existing uncertainties, including the tracer and CFC estimates (8 to 12 Sv) [*Jacobs et al.*, 1985; *Orsi et al.*, 1999], but not with the high estimate of *Sloyan and Rintoul* [2001]. Dianeutral diffusivities in the Southern Ocean are not resolved because of the weak constraints and limited parameterization of transformation processes.

7. Global Summary

[48] To present a very idealized summary of the integrated deep water fluxes for the period 1985–1996, mass transports are integrated on globally uniform, neutral surfaces (Figure 15). North Atlantic Deep Water is being produced in the northern North Atlantic and moved southward at a rate of 16 ± 2 Sv across 48°N. During its transit through the Atlantic Ocean, Antarctic Bottom Water and Antarctic Intermediate Waters are entrained, increasing the NADW transport to 23 ± 3 Sv as it exited the South Atlantic at 30°S. In the Southern Ocean, the dianeutral transports correspond to deep and bottom water transformations that are required by the global circulation. While the conversion of CDW into AAIW is rather uncertain with 8 ± 9 Sv, 21 ± 6 Sv of lower NADW is transformed into bottom water. Bottom water inflows to the Atlantic, Indian and Pacific

Table 7. Basin-Averaged Dianeutral Velocities and Diffusivities[a]

	W (Sv)	$\overline{w^*}$[b]	$\overline{\kappa^*}$[c]
Atlantic Deep[d]	3 ± 3	0.1 ± 0.05	3 ± 1.5
Indian Deep[d]	9 ± 5	0.3 ± 0.15	4 ± 2
Pacific Deep[d]	6 ± 4	0.1 ± 0.03	4 ± 1
Southern Deep[d]	14 ± 10	0.1 ± 0.1	–
Atlantic Bottom[e]	6 ± 2	0.5 ± 0.2	9 ± 4
Indian Bottom[e]	8 ± 4	0.6 ± 0.3	12 ± 7
Pacific Bottom[e]	7 ± 2.5	0.4 ± 0.1	9 ± 2
Southern Bottom[e]	−19 ± 6	−0.25 ± 0.1	–

[a]From *Ganachaud and Wunsch* [2000].
[b]10^{-6}m/s.
[c]10^{-4}m^2/s.
[d]γ^n = 27.96 to γ^n = 28.07 (2000 m to 3500 m).
[e]γ^n = 28.1 ($\simeq$3800 m) to the bottom.

Oceans are respectively 6 ± 1.3 Sv, 11 ± 4 Sv and 7 ± 2 Sv. In the Indian and Pacific Oceans, most of this water returns southward at deep and intermediate levels (transport values were slightly adjusted within uncertainties so that mass is strictly conserved in this global summary).

[49] The CDW inflow in the Indian Ocean contrasts with numerical model results summarized by *Zhang and Marotzke* [1999] that suggest weak inflow at depth. The most recent data assimilating models are reproducing strong overturning though (B. Ferron and J. Marotzke, Impact of 4-D variational assimilation of WOCE hydrography on the meridional circulation of the Indian Ocean, poster presented at WOCE and Beyond meeting, 19 Nov. 2002, San Antonio, Texas). In the North Pacific, the inflow of CDW is weaker than previously estimated as a consequence of the requirement of heat and salt conservation so most of the Pacific CDW upwells in the Tropical Pacific. A higher CDW inflow in the South Pacific would be possible only by relaxing PO conservation and tolerating increased mass imbalances. Because the bulk of the bottom water inflow returns at deep levels, the deep overturning cell is isolated, in the integrated sense, from the intermediate and surface water circulation.

[50] In the upper layers, a northward flow of thermocline water (16 ± 3 Sv at 48°N) from the South Atlantic Ocean balances the NADW southward flow; and the strength of Pacific-Indonesian-Through flow is estimated at 15 ± 5 Sv, in agreement with the most recent estimates. The South Pacific thermocline flow is directed northward, suggesting that the density class found in the Pacific-Indonesian Through flow ultimately originates in the South Pacific Ocean south of 32°S, although the exact pathway is complicated [*Fine et al.*, 1994; *Johnson and McPhaden*, 1999]. The horizontal structure of the flow for the density classes of Figure 15 (Figures 16a–16c) shows that while the direction of the integrated flow corresponds approximately to that suggested by traditional water mass analysis, it does not on small scales because of high variability or recirculations.

[51] Significant dianeutral exchanges are required by the global circulation (Table 7). Dianeutral velocities range 0.1–0.6 × 10^{-4} cm s^{-1} with largest upwelling values in the bottom layers. Large values are also found near the surface in regions of upwelling or downwelling. Diffusivities are 3–4 cm^2 s^{-1} in the deep layers, and higher near the bottom. Bottom water formation in the Southern Ocean

Table A1. North Atlantic Neutral Surface Layers[a]

Layer	Upper γ^n Interface	24°N (A5) Properties[b]	Water Mass Label
1	surface	(17.9)	Surface
2	26.44	$\sigma\theta = 26.40$; (15.8)	Thermocline
3	26.85	$\sigma\theta = 26.80$; (13.6)	
4	27.162	$\sigma\theta = 27.10$; (11.3)	
5	27.38	$\sigma\theta = 27.30$; (8.80)	Intermediate
6	27.62	$\sigma\theta = 27.50$; (6.90)	
7	27.82	$\sigma\theta = 27.70$; (5.20)	NADW[c]
8	27.922	$\sigma_2 = 36.87$; (3.60)	
9	27.975	$\sigma_2 = 36.94$; (3.20)	
10	28.008	$\sigma_2 = 36.98$; (3.00)	
11	28.044	$\sigma_2 = 37.02$; (2.76)	
12	28.072	$\sigma_4 = 45.81$; (2.50)	
13	28.0986	$\sigma_4 = 45.85$; (2.24)	
14	28.11	$\sigma_4 = 45.87$; (2.11)	
15	28.1295	$\sigma_4 = 45.90$; (1.93)	Bottom
16	28.141	$\sigma_4 = 45.91$; (1.85)	
17	28.154	$\sigma_4 = 45.92$; (1.81)	

[a]Layers are in kg m^{-3}.
[b]σ_x from *Macdonald* [1998, Table 11]: potential temperature in parentheses Macdonald changed the reference pressure when the potential density surface departed far from it. Her resulting layers consistently matched neutral surfaces, in contrast with the original σ layers which occasionally led to large departure from neutral surfaces, for example, a 500 dbar deviation was found near the Mediterranean waters.
[c]North Atlantic Deep Water.

corresponds to an average dianeutral velocity of $-0.25 \pm 0.1 \times 10^{-4}$ cm s^{-1} (diffusivities were not determined there). Between 30°S and 47°N, the global (area-weighted) average dianeutral velocity and diffusivity are of $\overline{w^*} = 0.13 \pm 0.03 \times 10^{-4}$ cm s^{-1} and $\overline{\kappa^*} = 3.7 \pm 0.7$ cm^2 s^{-1} in the deep range ($\simeq 2000 - 3000$ dbars). In the bottom layers (below 3500 dbars), larger values are found, with $\overline{w^*} = 0.4 \pm 0.1 \times 10^{-4}$ cm s^{-1} and $\overline{\kappa^*} = 9 \pm 2$ cm^2 s^{-1}. These values derive from a global tracer balance that includes all mixing processes, in particular the strong mixing generated near topography. *Munk and Wunsch* [1998] estimated an order of magnitude to the global value of 1 cm^2 s^{-1} from a crude one-dimensional global balance in the deep range. The

recent estimates of *Morris et al.* [2001] from in situ measurements and parameterized bottom roughness in the South Atlantic would rather suggest values of $1-5$ cm^2 s^{-1}. The fact that the global geostrophic circulation implies large mixing in the ocean interior is inconsistent with the suggestion that most mixing occurs near surface density outcrops, primarily in the Southern Ocean [*Toggweiler and Samuels*, 1998].

8. Discussion

[52] The linear model that we use represents one step toward producing an estimate of the oceanic circulation that is consistent globally, with ocean dynamics and biogeo-

Table A3. Southern Ocean Neutral Surface Layers[a]

Layer	Upper γ^n Interface	θ at 0°E 5.6°	Water Mass
1	surface	15	Surface
2	26.2	10	
3	26.8	4.3	AAIW
4	27.32	2.5	
5	27.57	1.7	UCDW
6	27.72	1.4	
7	27.903	1.5	LCDW[b]
8	28.03	1.45	
9	28.07	1	
10	28.15	0.6	
11	28.20	0.4	
12	28.23	0.15	
13	28.25	0	
14	28.27	−0.16	AABW[c]
15	28.296	−0.7	

[a]Same as Table A1. Partially based on the isopycnals of *Macdonald* [1998].
[b]The apparent temperature reversal between layers 7 and 8 is due to outcrop and salinity effects.
[c]The formal separation between AABW and CDW was taken at $\gamma^n = 28.27$, which corresponds to the sill depth of Drake Passage [*Orsi et al.*, 1999].

Table A2. Same as Table A1 but for the South Atlantic

Layer	Upper γ^n Interface	11°S (A8)θ	Water Mass Label[a]
1	surface	27	Surface
2	26.2	16.6	
3	26.8	11.8	
4	27.3	6.20	AAIW
5	27.5	4.30	Upper NADW
6	27.72	3.90	
7	27.903	3.70	
8	27.97	3.30	Middle NADW
9	28.03	2.75	
10	28.07	2.40	Lower NADW
11	28.11	2.00	AABW[b]
12	28.20	1.44	
13	28.23	0.60	
14	28.25	0.40	
15	28.27	0.22	
16	28.296	0.11	

[a]*Speer et al.* [1996] layer definitions are used. Water mass definitions are indicated [*Speer et al.*, 1996, Table 4].
[b]The nominal interface between NADW and AABW, $\gamma^n = 28.11$, remains close to $\theta = 2°$ between 30°S and 7°N, but varies from 1.4° to 1.8° at A11 (45°−30°S).

Table A4. Pacific Ocean Neutral Surface Layers[a]

Layer	Upper γ^n Interface	24°N $\sigma_x(\theta)$[b]	Water Mass
1	surface	$\sigma_\theta = 24.0(22.7)$	Surface
2	24.3	$\sigma_\theta = 24.3(21.9)$	
3	26	$\sigma_\theta = 26.0(12.6)$	NPIW
4	26.5	$\sigma_\theta = 26.4(9.1)$	
5	26.8	$\sigma_\theta = 26.7(7.1)$	
6	27	$\sigma_\theta = 26.9(5.9)$	
7	27.15	$\sigma_\theta = 27.0(5.2)$	
8	27.35	$\sigma_\theta = 27.2(4.4)$	AIW
9	27.6	$\sigma_2 = 36.56(3.5)$	
10	27.8	$\sigma_2 = 36.77(2.5)$	
11	27.9	$\sigma_2 = 36.88(2.0)$	
12	27.95	$\sigma_2 = 36.92(1.75)$	NPDW
13	28	$\sigma_2 = 36.97(1.5)$	
14	28.05	$\sigma_2 = 37.01(1.3)$	
15[c]	28.09	(1.15)	
16[c]	28.1	(1.10)	
17	28.11	$\sigma_4 = 45.885(1.06)$	CDW
18	28.125	$\sigma_4 = 45.900(1.02)$	
19	28.15	(0.85)	
20	28.18	(0.85)	

[a]Same as Table A1. The layers were suggested by J. Toole (personal communication, 1998), optimized to match the *Macdonald* [1998] layers and to keep similar thicknesses over the whole Pacific.
[b]The *Macdonald* [1998, Table 17] water mass definition are indicated.
[c]Interfaces 15 and 17 have been used in the North Pacific only.

Table B1. Atlantic Constraints Imposed on the Deep Layers by Bathymetric Features

Name	Section	Layer Depth[a]	Net Flux[b]	Longitude
Walvis R. North	A10	$\gamma^n = 28.11$ (4000)	0 ± 1 Sv	$7.3°W - 1.7°E$
Walvis R. South	A10	$\gamma^n = 28.11$ (4200)	0 ± 1 Sv	$2.2°E - 13.4°E$

Name	Box	Layer Depth	Net Div.[c]	Longitudes
East N. Atlantic	A2/A5	$\gamma^n = 28.0986$ (3500)	0 ± 3 Sv	$27°W - 11°W/45°W - 16°W$
East S. Atlantic 1	A8/A9	$\gamma^n = 28.11$ (4000)	0 ± 2 Sv	$13.2°W - 13.4°E/12.4°W - 10.8°E$
East S. Atlantic 2	A9/A10	$\gamma^n = 28.11$ (4000)	0 ± 2 Sv	$12.4°W - 10.8°E/13.6°W - 14.7°E$
East S. Atlantic 3	A10/A11	$\gamma^n = 28.20$ (4500)	0 ± 2 Sv	$13.6°W - 14.7°E/15°W - 15.6°E$

[a]Layer and depth below which the flux is constrained.
[b]Constraints on the net flux through a single section for a longitude range (positive northward).
[c]Constraints on the net divergence in a box between two sections.

chemical cycles. Such a time-average model permits the estimation of meridional property transports from the highest resolution allowed by hydrographic data and, more importantly, permits estimation of the true uncertainties. The circulation, transports and diffusivities provide a reference for climate studies, for instance as a way to test general circulation models and parameterize the sub-grid-scale processes. The associated heat and freshwater transfers are discussed separately [*Ganachaud and Wunsch*, 2003c], as are the analyses of nutrient and oxygen [*Ganachaud and Wunsch*, 2002] that provide estimates for export production and atmospheric oxygen exchanges. The circulation in the Atlantic Ocean is remarkably close to estimates obtained from previous data, suggesting little change in integrated mass transports over the past 30 years. In the Pacific Ocean, the net deep inflow is weaker than previous estimates, and the difference seems to be caused by our different constraints [*Roemmich and McCallister*, 1989; *Macdonald*, 1998]. A stringent test for detection of changes would be to produce an estimate of the circulation from earlier data using the same treatment and model as used here.

[53] A time-averaged budget relies upon an ergodic hypothesis, that large-scale quantities are close to the time mean, and the remaining uncertainty is dominated by oceanic variability in the density and other properties. For example, the property transports in the Indonesian Throughflow and the North Brazil Current are a large source of uncertainty, because of the lack of measurements

and the large seasonality. The uncertainties that we report include both the model limitations and the measurements errors, with the impact of ocean variability being accounted for by reference to a general circulation model simulation [*Ganachaud*, 2003]. A standard, or preferred solution is selected among a large number of experiments (about 100 in total), and there is no limit to possible configurations of the model. Detailed regional studies will help improve the model consistency by further adjustments to the initial reference surface and by use of additional data to eventually reduce the residual uncertainty in the solutions [e.g., *Wijffels et al.*, 2001]. Our experiments suggested that large-scale mass transports after inversion are relatively insensitive to the reference surfaces [e.g., *Ganachaud et al.*, 2000]; nevertheless, a straightforward way toward improvement is a formal combination of the ongoing regional analyses through collaborative work and gathering of regional results to produce a globally consistent estimate.

[54] Because, in linear models, variability in the density field is a major source of uncertainty, the impact of new data is necessarily limited. Simple steady state (or time-average) models with corrections to the density field have been used in the past [*Wunsch*, 1994], and the major obstacle, apart from computational load, is the lack of knowledge about a priori statistics for the density variability. Data assimilation in general circulation models is the natural way toward ocean circulation estimation. Computer capabilities are

Table B2. Pacific Constraints Imposed on the Deep Layers by Bathymetric Features

Name	Section	Layer Depth	Net Flux	Longitude
N. Tasmanian	P21W	$\gamma^n = 28.1$ (3900)	0 ± 2 Sv	$153°E - 156°E$
S. NewCal Trough	P6	$\gamma^n = 27.9$ (2000)	0 ± 2 Sv	$162°E - 168°E$
Yupanqui Basin[a]	P21	$\gamma^n = 28.05$ (3700)	0 ± 5 Sv	$94°W - 78°W$
Bauer Basin	P21	$\gamma^n = 28.05$ (3900)	0 ± 2 Sv	$107°W - 100°W$
N. Peru Basin	P21	$\gamma^n = 28.05$ (3900)	0 ± 2 Sv	$94°W - 75°W$
Okinawa Trough	P3	$\gamma^n = 27.6$ (1200)	0 ± 2 Sv	$125°E - 127°E$
N. Philippines Bas.	P3	$\gamma^n = 28.05$ (3100)	0 ± 2 Sv	$127°E - 141°E$
Kuril Trench	P1	$\gamma^n = 28.11$ (4900)	0 ± 2 Sv	$145°E - 147°E$

Name	Box	Layer Depth	Net Div.	Longitudes
Tasmanian	P6/P21W	$\gamma^n = 28.1$ (3900)	0 ± 2 Sv	$153°E - 157°E/153°E - 156°E$
NewCal Trough	P6/P21W	$\gamma^n = 27.9$ (2000)	0 ± 2 Sv	$162°E - 168°E/162°E - 164°E$
S. Fiji Basin	P6/P21	$\gamma^n = 28.0$ (2700)	0 ± 2 Sv	$173°E - 179°E/165°E - 168°E$
South West Basin[a]	P6/P21	$\gamma^n = 28.05$ (3600)	0 ± 5 Sv	$179°W - 122°W/173°W - 114°W$
Peru-Chile Basin[a]	P6/P21	$\gamma^n = 28.05$ (3900)	0 ± 5 Sv	$112°W - 71°W/77°W - 75°W$

[a]A relatively large tolerance of ± 5 Sv was given to the South West Basin, Yupanqui Basin ($20°S - 105°W$), and Peru-Chile Basin to allow dianeutral exchanges with layers above.

Table C1. Initial Ekman Transport[a] and Correction[b]

Section	Initial	Final	Correction, %
A2	−2.7 ± 1	−2.7 ± 1	0
Florida Strait	0	0	−
A5	+4.6 ± 2	3 ± 1.7	−32
A6	+8.2 ± 4	8.3 ± 3.6	1
A7	−17 ± 8	−19 ± 6.8	13
A8	−10 ± 5	−8.6 ± 4	−14
A9	−5.5 ± 3	−6.3 ± 2.6	13
A10	−0.5 ± 1	−0.6 ± 1	−
A11	+6 ± 3	5.8 ± 2.8	−3
A21	0.06 ± 1	0 ± 1	−
A12	−1.3 ± 1	−1.4 ± 1	1
I6	0.6 ± 1	0.6 ± 1	0%
I9S	−0.9 ± 1	−0.9 ± 1	−
P12	0 ± 1	0 ± 0.5	−
P14S	−0.5 ± 1	−0.46 ± 1	−
P6	1.4 ± 1	1.3 ± 1	−10
P21	−18 ± 8	−20 ± 6	15
P3	7.5 ± 3	9 ± 3	13%
P1	−4 ± 2	−3.9 ± 1.6	−3
I5	0.3 ± 1	0.5 ± 1	−
I4	−0.5 ± 1	−0.5 ± 1	−
I3	−11.5 ± 5	−10 ± 4	−8
I2W	−4.5 ± 20	9 ± 10	−300
I2	−11.6 ± 5	−11 ± 5	−6
I10	−2.9 ± 1	−2.9 ± 1	0
J89	−0.65 ± 1	−0.6 ± 1	−

[a]In sverdrups, positive eastward or northward.
[b]The correction applies to the change in the first layer of the model, including Ekman, geostrophic, and ageostrophic processes.

currently limiting the resolution and prohibiting calculation of uncertainties, and the ongoing efforts, in parallel with simple statistical estimates such as the one presented here, will keep converging toward estimating the time-varying ocean circulation.

[55] Dianeutral exchanges are also poorly parameterized in regions of outcrop such as the Southern Ocean. There, an advection-diffusion scheme is unrealistic, and allowing independent transports for each property may be necessary [*Sloyan and Rintoul*, 2000]. The possibility of double diffusion was not addressed. *You* [2000] highlighted its importance in the North Indian Ocean for instance. Using distinct diffusion coefficients for heat and salt could be explored. The parameterization of *Sloyan and Rintoul* [2000] attack that problem although it may leave too much freedom in vertical exchanges, as discussed above. Last, the a priori statistics can be improved. For instance, the weight of anomaly equations can be estimated from a simulation by a general circulation model as was done for the mass transports, instead of the ad-hoc weights that we used. Variability in the nutrient transports is another major error source that could not be quantified. Repeat survey will provide useful insights for such variability, would the measurement be made only over the upper layers that are the most sensitive to seasonal cycle. The standard model results can be downloaded from http://puddle.mit.edu/ganacho/glbwocemodel.html.

Appendix A: Layer and Water Mass Definition

[56] Tables A1−A4: layer interfaces (neutral surfaces) that were chosen to impose conservation constraints and diagnose transports.

Appendix B: Bathymetric Constraints

[57] Tables B1−B2 describe the constraints imposed on the deep layer transports by bathymetric features.

Appendix C: Ekman Transports

[58] The average wind stress of the NCEP/NCAR reanalysis [*Kalnay et al.*, 1996] over the period 1992 to 1997 is used to compute the initial Ekman transport (Table C1). This period does not exactly overlap with the hydrographic data. The model-derived correction to the Ekman transport is assumed to accommodate the temporal differences. The final "Ekman" transport represents the total change made to the flow in the surface layers, including all ageostrophic processes and adjustments to the initial geostrophic transport. The initial Ekman transports are tiny in the Southern Ocean and a minimum uncertainty ±1 Sv was attributed. Because of the large baroclinic variability in the East African Coastal Current (EACC) on section I2W, a large adjustment (±20 Sv) was allowed to the flow in the first layer. Relatively small adjustments were made to the initial NCEP Ekman transports, except in I2W (300%) in the Mozambique Channel where the variability in the baroclinic transports is large.

References

Anderson, L. A., and J. L. Sarmiento, Redfield ratios of remineralization determined by nutrient data analysis, *Global Biogeochem. Cycles*, *8*, 65–85, 1994.

Arhan, M., H. Mercier, B. Bourles, and Y. Gouriou, Two hydrographic sections across the Atlantic at 7°30N and 4°30S, *Deep Sea Res., Part I*, *45*, 826–872, 1998.

Banks, H., J. Bullister, S. Bacon, H. Bryden, and J. Rennell, The deep western boundary current at 17°S in the Pacific Ocean, *Int. WOCE Newsl.*, *19*, 3–5, 1995.

Beal, L. M., and H. L. Bryden, Observation of an Agulhas undercurrent, *Deep Sea Res., Part I*, *44*, 1715–1724, 1997.

Bray, N. A., S. E. Wijffels, J. C. Chong, M. Fieux, S. Hautala, G. Meyers, and W. M. L. Morawitz, Characteristics of the Indo-Pacific Throughflow in the eastern Indian Ocean, *Geophys. Res. Lett.*, *24*, 2569–2572, 1997.

Broecker, W. S., "NO", a conservative water-mass tracer, *Earth Planet. Sci. Lett.*, *23*, 100–107, 1974.

Broecker, W. S., S. Sutherland, and T.-H. Peng, A possible 20th-century slowdown of Southern Ocean deep water formation, *Science*, *286*, 1132–1135, 1999.

Chiswell, S. M., J. Toole, and J. Church, Transports across the Tasman Sea from WOCE repeat sections: The East Australian Current 1990–94, *N. Z. J. Mar. Freshwater Res.*, *31*, 469–475, 1997.

Clarke, R. A., R. M. Hendry, I. Yashayaev, and D. R. Watts, A western boundary current array in the North Atlantic near 42°N, *Int. WOCE Newsl.*, *33*, 33–34, 1998.

Coachman, L. K., and K. Aagaard, Transports through the Bering Strait: Annual and interannual variability, *J. Geophys. Res.*, *93*, 15,535–15,539, 1988.

Coatanoan, C., N. Metzl, M. Fieux, and B. Coste, Seasonal water mass distribution in the Indonesian Throughflow entering the Indian Ocean, *J. Geophys. Res.*, *104*, 20,801–20,826, 1999.

de las Heras, M., and R. Schlitzer, On the importance of intermediate water flows for the global ocean overturning, *J. Geophys. Res.*, *104*, 15,515–15,536, 1999.

DeRuijter, W., H. Ridderinkhof, J. Lutjeharms, M. Schouten, and C. Veth, Observations of the flow in the Mozambique Channel, *Geophys. Res. Lett.*, *29*(10), 1502, doi:10.1029/2001GL013714, 2002.

DiMarco, S., P. Chapman, W. Nowlin, P. Hacker, K. Donohue, M. Luther, G. Johnson, and J. Toole, Volume transport and property distributions of the Mozambique Channel, *Deep Sea Res., Part I*, *49*, 1481–1511, 2002.

Donohue, K., and J. Toole, A near-synoptical survey of the southwest Indian Ocean, *Elsevier Sci.*, in press, 2003.

Fieux, M., C. Andrié, P. Delecluse, A. G. Ilaude, A. Kartavtseff, F. Mantisi, R. Molcard, and J. C. Swallow, Measurements within the Pacific-Indian Oceans Through flow region, *Deep Sea Res., Part I*, *41*, 1091–1130, 1994.

Fine, R. A., R. Lukas, M. Bingham, M. J. Warner, and R. H. Gammon, The western equatorial Pacific: A water mass crossroads, *J. Geophys. Res.*, *99*, 25,063–25,080, 1994.

Fu, L. L., Mass, heat and freshwater fluxes in the south Indian Ocean, *J. Phys. Oceanogr.*, *16*, 1683–1693, 1986.

Ganachaud, A., Large scale oceanic circulation and fluxes of freshwater, heat, nutrients and oxygen, Ph.D. thesis, 267 pp., Mass. Inst. of Technol./ Woods Hole Oceanogr. Inst. Joint Program, Cambridge, 1999.

Ganachaud, A., Error budget of inverse box models: The North Atlantic, *J. Atmos. Oceanic Technol.*, in press, 2003.

Ganachaud, A., and C. Wunsch, The oceanic meridional overturning circulation, mixing, bottom water formation and heat transport, *Nature*, *408*, 453–457, 2000.

Ganachaud, A., and C. Wunsch, Oceanic nutrient and oxygen transports and bounds on export production during the World Ocean Circulation Experiment, *Global Biogeochem. Cycles*, *16*(4), 1057, doi:10.1029/ 2000GB001333, 2002.

Ganachaud, A., and C. Wunsch, Large scale ocean heat and freshwater transports during the World Ocean Circulation Experiment, *J. Clim.*, *16*, 696–705, 2003.

Ganachaud, A., C. Wunsch, J. Marotzke, and J. Toole, The meridional overturning and large-scale circulation of the Indian Ocean, *J. Geophys. Res.*, *105*, 26,117–26,134, 2000.

Garzoli, S. L., A. L. Gordon, V. Kamenkovich, D. Pillsbury, and C. Dun-combeRae, Variability and sources of the southeastern Atlantic circulation, *J. Mar. Res.*, *54*, 1039–1071, 1996.

Gordon, A. L., R. D. Susanto, and A. Ffield, Throughflow within the Makassar Strait, *Geophys. Res. Lett.*, *26*, 3325–3328, 1999.

Hall, M. M., and H. L. Bryden, Direct estimates and mechanisms of ocean heat transport, *Deep Sea Res., Part A*, *29*, 339–359, 1982.

Hall, M. M., M. McCartney, and J. A. Whitehead, Antarctic Bottom Water flux in the equatorial western Atlantic, *J. Phys. Oceanogr.*, *27*, 1903–1926, 1997.

Hogg, N. G., and W. B. Owens, Direct measurements of the deep circulation within the Brazil Basin, *Deep Sea Res., Part II*, *46*, 335–353, 1999.

Hogg, N., P. Biscaye, W. Gardner, and W. J. Schmitz Jr., On the transport and modification of Antarctic Bottom Water in the Vema Channel, *J. Mar. Res.*, *40*, suppl., 231–263, 1982.

Hogg, N. G., G. Siedler, and W. Zenk, Circulation and variability at the southern boundary of the Brazil Basin, *J. Phys. Oceanogr.*, *29*, 145–157, 1999.

Holfort, J., and G. Siedler, The meridional oceanic transports of heat and nutrients in the South Atlantic, *J. Phys. Oceanogr.*, *31*, 5–29, 2001.

Hufford, G. E., M. S. McCartney, and K. A. Donohue, Northern boundary currents and adjacent recirculations off southwestern Australia, *Geophys. Res. Lett.*, *24*, 2797–2800, 1997.

Ichikawa, H., and R. C. Beardsley, Temporal and spatial variability of volume transport of the Kuroshio in the East China Sea, *Deep Sea Res., Part I*, *40*, 583–605, 1993.

Jackett, D. R., and T. J. McDougall, A neutral density variable for the world's oceans, *J. Phys. Oceanogr.*, *27*, 237–263, 1997.

Jacobs, S. S., R. G. Fairbanks, and Y. Horibe, Origin and evolution of water masses near the Antarctic continental margin, in *Oceanology of the Antarctic Continental Shelf*, *Antarct. Res. Ser.*, vol. 43, edited by S. S. Jacobs, pp. 59–85, AGU, Washington, D. C., 1985.

Johns, W. E., T. N. Lee, R. C. Beardsley, J. Candela, R. Limeburner, and B. Castro, Annual cycle and variability of the North Brazil Current, *J. Phys. Oceanogr.*, *28*, 103–128, 1998.

Johnson, G. C., The Pacific Ocean subtropical cell surface limb, *Geophys. Res. Lett.*, *28*, 1771–1774, 2001.

Johnson, G. C., and M. J. McPhaden, Interior pycnocline flow from the subtropical to the squatorial Pacific Ocean, *J. Phys. Oceanogr.*, *29*, 3037–3089, 1999.

Johnson, G. C., and J. M. Toole, Flow of deep and bottom waters in the Pacific at 10°N, *Deep Sea Res., Part I*, *40*, 371–394, 1993.

Johnson, G. C., D. L. Musgrave, B. A. Warren, A. Ffield, and D. B. Olson, Flow of bottom and deep water in the Amirante Passage and Mascarene basin, *J. Geophys. Res.*, *103*, 30,973–30,984, 1998.

Johnson, G. C., M. J. McPhaden, and E. Firing, Equatorial Pacific Ocean horizontal velocity, divergence and upwelling, *J. Phys. Oceanogr.*, *31*, 839–849, 2001.

Kalnay, E., et al., P/NCAR 40-year reanalysis project, *Bull. Am. Meteorol. Soc.*, *77*, 437–471, 1996.

Kawai, H., Hydrography of the Kuroshio extention, in *Kuroshio: Its Physical Aspects*, edited by H. Stommel and K. Yoshida, pp. 335–352, Univ. of Tokyo Press, Tokyo, 1972.

Koltermann, K. P., A. Sokov, V. Terechtchencov, S. Dobroliubov, K. Lorbacher, and A. Sy, Decadal changes in the thermohaline circulation of the North Atlantic, *Deep Sea Res., Part II*, *46*, 109–138, 1999.

Ledwell, J., A. Watson, and C. Law, Mixing of a trace released in the thermocline, *J. Geophys. Res.*, *103*, 21,499–21,529, 1998.

Ledwell, J., E. Montgomery, K. Polzin, L. S. Laurent, R. Schmitt, and J. Toole, Evidence for enhanced mixing over rough topography in the abyssal ocean, *Nature*, *403*, 179–182, 2000.

Lee, T., and J. Marotzke, Seasonal cycles of meridional overturning and heat transport of the Indian Ocean, *J. Phys. Oceanogr.*, *28*, 923–943, 1998.

Lemke, P., The expedition Antarktis X/4 of RV *Polarstern* in 1992, *Ber. Polarforschung 140*, 90 pp., Alfred-Wegener-Inst. für Merresforsch., Bremerhaven, Germany, 1994.

Levitus, S., and T. P. Boyer, *World Ocean Atlas 1997*, vol. 4, *Temperature*, *NOAA Atlas NESDIS*, vol. 4, 129 pp., Natl. Oceanic and Atmos. Admin., Silver Spring, Md., 1994.

Levitus, S., R. Burgett, and T. Boyer, *World Ocean Atlas 1994*, vol. 3, *Salinity*, *NOAA Atlas NESDIS*, vol. 3, Natl. Oceanic and Atmos. Admin., Silver Spring, Md., 1994.

Lux, M., Franchissement de l'Equateur par les masses d'eau dans le cadre de la circulation thermohaline, Ph.D. thesis, Lab. de Phys. des Océans, Univ. de Bretagne Occidentale, Inst. Fr. de Rech. Pour l'Exploit de la Mer Cent. de Brest, Plouzané, 1997.

Lux, M., and H. Mercier, Interhemispheric exchanges of mass and heat in the Atlantic Ocean in January–March 1993, *Deep Sea Res., Part I*, *48*, 605–638, 2001.

Macdonald, A., Oceanic fluxes of mass, heat and freshwater: A global estimate and perspective, Ph.D. thesis, Mass. Inst. of Technol./Woods Hole Oceanogr. Inst. Joint Program, Cambridge, 1995.

Macdonald, A., The global ocean circulation: A hydrographic estimate and regional analysis, *Prog. Oceanogr.*, *41*, 281–382, 1998.

Macdonald, A. M., and C. Wunsch, An estimate of global ocean circulation and heat fluxes, *Nature*, *382*, 436–439, 1996.

McCartney, M. S., and R. A. Curry, Transequatorial flow of Antarctic Bottom Water in the western Atlantic Ocean: Abyssal geostrophy at the equator, *J. Geophys. Res.*, *23*, 1264–1276, 1993.

McDougall, T. J., Dianeutral advection, paper presented at Parameterization of Small-Scale Processes Hawaiian Winter Workshop, Univ. of Hawaii at Manoa, Honolulu, 1991.

McTaggart, K. E., and G. C. Johnson, CTD/O2 measurements collected on a Climate and Global Change cruise (WOCE sections P14S and P15S) during January–March 1996, *NOAA Data Rep., ERL PMEL-63*, 485 pp., 1997. (Available at http://jelly.pmel.noaa.gov/admin/scripts/Publications. asp?ABSTRACT_REQUEST=1895.)

Mensch, M., R. Bayer, J. Bullister, P. Schlosser, and R. Weiss, The distribution of tritium and CFCs in the Weddell Sea during the mid-1980s, *Prog. Oceanogr.*, *38*, 377–415, 1996.

Mercier, H., and K. Speer, Transport of bottom water in the Romanche Fracture Zone and the Chain Fracture Zone, *J. Phys. Oceanogr.*, *28*, 779–790, 1998.

Morris, M., M. Hall, L. S. Laurent, and N. Hogg, Abyssal mixing in the Brazil Basin, *J. Phys. Oceanogr.*, *31*, 3331–3348, 2001.

Muller, T. J., Y. Ideka, N. Zangenberg, and L. V. Nonato, Direct measurements of western boundary currents off Brazil between 20°S and 28°S, *J. Geophys. Res.*, *103*, 5429–5437, 1998.

Munk, W., and C. Wunsch, The Moon and mixing: Abyssal recipes II, *Deep Sea Res., Part I*, *45*, 1977–2010, 1998.

Orsi, A. H., G. C. Johnson, and J. L. Bullister, Circulation, mixing and production of Antarctic Bottom Water, *Prog. Oceanogr.*, *43*, 55–109, 1999.

Orsi, A. H., S. Jacobs, A. Gordon, and M. Visbeck, Cooling and ventilation the abyssal ocean, *Geophys. Res. Lett.*, *28*, 2923–2926, 2001.

Oudot, C., P. Morin, F. Baurand, M. Wafar, and P. L. Corre, Northern and southern water masses in the equatorial Atlantic sector: Results of nutrients from the CITHER-1 cruise (WOCE A6 and A7 lines), *Deep Sea Res., Part I*, *45*, 873–902, 1998.

Parilla, G., A. Lavin, H. Bryden, M. Garcia, and R. Millard, Rising temperature in the subtropical North Atlantic over the past 35 years, *Nature*, *369*, 48–51, 1994.

Park, Y.-H., E. Charriaud, P. Craneguy, and A. Kartavtseff, Fronts, transports, and Weddell Gyre at 30°E between Africa and Antarctica, *J. Geophys. Res.*, *106*, 2857–2879, 2001.

Polzin, K. L., J. M. Toole, G. R. Ledwell, and R. W. Schmitt, Spatial variability of turbulent mixing in the abyssal ocean, *Science*, *276*, 93–96, 1997.

Redfield, A. C., B. H. Ketchum, and F. A. Richards, The influence of organisms on the composition of sea water, in *The Sea*, vol. 2, edited by M. N. Hill, pp. 26–77, Wiley-Interscience, New York, 1963.

Reid, J., *Intermediate Waters of the Pacific Ocean, Johns Hopkins Oceanogr. Stud.*, vol. 2, Johns Hopkins Press, Baltimore, Md., 1965.

Reid, J., On the total geostrophic circulation of the North Atlantic Ocean: Flow patterns, tracers, and transports, *Prog. Oceanogr.*, *33*, 1–92, 1994.

Reid, J., On the circulation of the South Atlantic Ocean, in *The South Atlantic: Past and Present Circulation*, edited by G. Wefer et al., pp. 13–44, Springer, New York, 1996.

Richardson, P. L., and W. Schmitz, Deep cross-equatorial flow in the Atlantic measured with SOFAR floats, *J. Geophys. Res.*, *98*, 8371–8387, 1993.

Riley, G. A., Oxygen, phosphate and nitrate in the Atlantic Ocean, *Bull. Bingham Oceanogr. Collect.*, *12*, 169 pp., 1951.

Rintoul, S. R., South Atlantic inter basin exchange, *J. Geophys. Res.*, *96*, 2592–2675, 1991.

Rintoul, S. R., On the origin and influence of Adélie Land bottom water, in *Ocean, Ice and Atmosphere: Interactions at the Antarctic Continental Margin, Antarct. Res. Ser.*, vol. 75, edited by S. Jacobs and R. Weiss, pp. 151–171, AGU, Washington, D. C., 1998.

Rintoul, S. R., and J. L. Bullister, A late winter hydrographic section from Tasmania to Antarctica, *Deep Sea Res., Part I*, *46*, 1417–1454, 1999.

Rintoul, S. R., and C. Wunsch, Mass, heat, oxygen and nutrient fluxes and budget in the North Atlantic Ocean, *Deep Sea Res., Part A*, *38*, 355–377, 1991.

Robbins, P. E., and J. M. Toole, The dissolved silica budget as a constraint on the meridional overturning circulation in the Indian Ocean, *Deep Sea Res., Part I*, *44*, 879–906, 1997.

Roemmich, D., and T. McCallister, Large scale circulation of the North Pacific Ocean, *Prog. Oceanogr.*, *22*, 171–204, 1989.

Roemmich, D., and C. Wunsch, Two transatlantic sections: Meridional circulation and heat flux in the subtropical North Atlantic Ocean, *Deep Sea Res., Part A*, *32*, 119–664, 1985.

Roemmich, D., S. Hautala, and D. Rudnick, Northward abyssal transport through the Samoan passage and adjacent regions, *J. Geophys. Res.*, *101*, 14,039–14,055, 1996.

Roether, W., R. Schlitzer, A. Putzka, P. Beining, K. Bulsiewicz, G. Rohardt, and F. Delahoyde, A chlorofluoromethane and hydrographic section across Drake Passage-Deep water ventilation and meridional property transport, *J. Geophys. Res.*, *98*, 14,423–14,435, 1993.

Rosenberg, M., S. Bray, N. Bindoff, S. Rintoul, N. Johnson, S. Bell, and P. Towler, Aurora Australis Marine Science Cruises AU9501, AU9604 and AU9601-Oceanographic field measurements and analysis, intercruise comparisons and data quality notes, *Tech. Rep. 12*, Antarct. Coop. Res. Cent., Hobart, Tasmania, Aust., 1997.

Saunders, P. M., and B. B. King, Oceanic fluxes on the WOCE A11 section, *J. Phys. Oceanogr.*, *25*, 1942–1958, 1995.

Schmitz, W., On the world ocean circulation, vol. I, Some global features/North Atlantic Circulation, *Tech. Rep. WHOI-96-03*, Woods Hole Oceanogr. Inst., Woods Hole, Mass., 1996.

Schmitz, W., and M. S. McCartney, On the North Atlantic circulation, *Rev. Geophys.*, *31*, 29–49, 1993.

Schott, F. A., and J. P. McCreary, Transports and pathways of the upper-layer circulation in the western tropical Atlantic, *Prog. Oceanogr.*, *51*, 1–123, 2001.

Schott, F. A., T. N. Lee, and R. Zantopp, Variability of structure and transport of the Florida Current in the period range of day to seasonal, *J. Phys. Oceanogr.*, *18*, 1209–1230, 1988.

Shriver, J. F., and H. E. Hulburt, The contribution of the global thermohaline circulation to the Pacific and Indian Throughflow via Indonesia, *J. Geophys. Res.*, *102*, 5491–5511, 1997.

Siedler, G., T. J. Mueller, R. Onken, M. Arhan, H. Mercier, B. A. King, and P. M. Saunders, The zonal WOCE sections in the South Atlantic, in *The South Atlantic: Past and Present Circulation*, edited by G. Wefer et al., pp. 83–104, Springer-Verlag, New York, 1996.

Sloyan, B. M., and S. R. Rintoul, Estimates of area-averaged diapycnal fluxes from basin-scale budgets, *J. Phys. Oceanogr.*, *30*, 2320–2341, 2000.

Sloyan, B. M., and S. R. Rintoul, The Southern Ocean limb of the global deep overturning circulation, *J. Phys. Oceanogr.*, *31*, 143–173, 2001.

Speer, K. G., J. Holfort, T. Reynaud, and G. Siedler, South Atlantic heat transport at 11°S, in The South Atlantic: Past and Present Circulation, edited by G. Wefer et al., pp. 105–120, Springer, New York, 1996.

Sprintall, J., S. Wijffels, T. Chereskin, and N. Bray, The JADE and WOCE I10/IR6 Throughflow sections in the southeast Indian Ocean. part 2: velocity and transports, *Deep Sea Res., Part II*, *49*, 1363–1390, 2002.

Stommel, H., and A. B. Arons, On the abyssal circulation of the world ocean-IAn idealized model of the circulation pattern and amplitude in oceanic basins, *Deep Sea Res.*, *6*, 217–233, 1960.

Stommel, H., E. D. Stroup, and B. Warren, Trans-Pacific hydrographic sections at lats. 43°S and 28°S: The *Scorpio* expedition-I. Preface, *Deep Sea Res.*, *20*, 1–7, 1973.

Talley, L., Some aspects of ocean heat transport by the shallow, intermediate and deep overtuning circulations, in *Mechanisms of Global Climate Change at Millenial Time Scales, Geophys Monogr. Ser.*, vol. 112, edited by P. U. Clark, R. S. Webb, and L. D. Keigwin, pp. 1–22, AGU, Washington, D. C., 1999.

Talley, L., Shallow, intermediate and deep overturning components of the global heat budget, *J. Phys. Oceanogr.*, *33*, 530–560, 2003.

Talley, L. D., and D. Roemmich (Eds.), Joseph L. Reid: A tribute in recognition of 40 years of contribution to oceanography, *Deep Sea Res., Part A*, *38*, suppl., 654 pp., 1991.

Toggweiler, J. R., and B. Samuels, On the ocean's large-scale circulation near the limit of no vertical mixing, *J. Phys. Oceanogr.*, *28*, 1832–1852, 1998.

Toole, J., and B. A. Warren, A hydrographic section across the subtropical south Indian Ocean, *Deep Sea Res., Part I*, *40*, 1973–2019, 1993.

Tsimplis, M. N., S. Bacon, and H. L. Bryden, The circulation of the subtropical South Pacific derived from hydrographic data, *J. Geophys. Res.*, *103*, 21,443–21,468, 1998.

Warner, M. J., and G. I. Roden, Chlorofluorocarbon evidence for recent ventilation of the deep Bering Sea, *Nature*, *373*, 409–412, 1995.

Warren, B. A., Transpacific sections at lats. 43°S and 28°N: The *Scorpio* expedition-I. I. Deep water, *Deep Sea Res.*, *20*, 9–38, 1973.

Warren, B. A., Why is no deep water formed in the North Pacific?, *J. Mar. Res.*, *41*, 327–341, 1983.

Weatherly, G. L., Y. Y. Kim, and E. A. Kontar, Eulerian measurements of the North Atlantic Deep Water deep western boundary current at 18°S, *J. Phys. Oceanogr.*, *30*, 971–986, 2000.

Whitworth, T., W. Nowlin, and S. J. Worley, The net transport of the Antarctic Circumpolar Current through Drake Passage, *J. Phys. Oceanogr.*, *12*, 960–971, 1982.

Whitworth, T., B. A. Warren, W. D. Nowlin Jr., S. B. Rutz, R. D. Pillsbury, and M. I. Moore, On the deep western-boundary current in the Southwest Pacific Basin, *Prog. Oceanogr.*, *43*, 1–54, 1999.

Wijffels, S. E., Exchanges between hemispheres and gyres: A direct approach to the mean circulation of the equatorial Pacific, Ph.D. thesis, 297 pp., Mass. Inst. of Technol./Woods Hole Oceanogr. Inst. Joint Program, Cambridge, 1993.

Wijffels, S. E., J. M. Toole, H. L. Bryden, R. A. Fine, W. J. Jenkins, and J. L. Bullister, The water masses and circulation at 10°N in the Pacific, *Deep Sea Res., Part I*, *43*, 501–544, 1996.

Wijffels, S. E., J. M. Toole, and R. Davis, Revisiting the South Pacific subtropical circulation: A synthesis of WOCE observations along 32°S, *J. Geophys. Res.*, *106*, 19,481–19,513, 2001.

Worthington, L. V., and H. Kawai, Comparison between deep sections across the Kuroshio and the Florida Current and Gulf Stream, in *Kuroshio: Its Physical Aspects*, edited by H. Stommel and K. Yoshida, pp. 371–386, Univ. of Tokyo Press, Tokyo, 1972.

Wunsch, C., The North Atlantic general circulation West of 50°W determined by inverse methods, *Rev. Geophys.*, *16*, 583–620, 1978.

Wunsch, C., Dynamically consistent hydrography and absolute velocity in the eastern North Atlantic Ocean, *J. Geophys. Res.*, *99*, 14,071–14,090, 1994.

Wunsch, C., *The Ocean Circulation Inverse Problem*, 437 pp., Cambridge Univ. Press., New York, 1996.

Wunsch, C., and B. Grant, Towards the general circulation of the North Atlantic Ocean, *Prog. Oceanogr.*, *11*, 1–59, 1982.

Wunsch, C., D. Hu, and B. Grant, Mass, heat, salt and nutrient fluxes in the South Pacific Ocean, *J. Phys. Oceanogr.*, *13*, 725–753, 1983.

You, Y., Contribution of salt-fingering to the conveyor belt circulation in the abyssal northern Indian Ocean, *Geophys. Res. Lett.*, *27*, 3913–3916, 2000.

Zemba, J. C., The structure and transport of the Brazil Current between 27° and 36° south, Ph.D. thesis, 160 pp., Woods Hole Oceanogr. Inst./Mass. Inst. of Technol., Woods Hole, 1991.

Zenk, W., G. Siedler, B. Lenz, and N. G. Hogg, Antarctic Bottom Water flow through the Hunter Channel, *J. Phys. Oceanogr.*, *29*, 2785–2801, 1999.

Zhang, D., T. N. Lee, W. E. Johns, C.-T. Liu, and R. Zantopp, The Kuroshio east of Taiwan: Modes of variability and relationship to interior ocean mesoscale eddies, *J. Phys. Oceanogr.*, *31*, 1054–1074, 2001.

Zhang, K. Q., and J. Marotzke, The importance of open-boundary estimation for an Indian Ocean GCM-data synthesis, *J. Mar. Res.*, *57*, 305–334, 1999.

————————————
A. Ganachaud, Institut de Recherche pour le Développement, Laboratoire d'Etudes Géophysiques et d'Océautographie Spatiale, BP A5, Nouméa, New Caledonia. (Alexandre.Ganachaud@noumea.ird.fr)